

Article

The Geology and Mineral Chemistry of Beryl Mineralization, South Eastern Desert, Egypt: A Deeper Insight into Genesis and Distribution

Mohamed Zaki Khedr ^{1,*}, Gehad M. Saleh ², Khaled M. Abdelfadil ³, Eiichi Takazawa ⁴, Kamal Abdelrahman ⁵, Akihiro Tamura ⁶ and Shaimaa Ali El-Shafei ⁷

¹ Geology Department, Faculty of Science, Kafrelsheikh University, Kafr El-Sheikh 33516, Egypt

² Nuclear Materials Authority, P.O. Box 530, El-Maadi, Cairo 11728, Egypt

³ Department of Geology, Faculty of Science, Sohag University, Sohag 82524, Egypt

⁴ Geology Department, Faculty of Science, Niigata University, Niigata 950-2181, Japan; takazawa@geo.sc.niigata-u.ac.jp

⁵ Department of Geology and Geophysics, College of Science, King Saud University, P.O. Box 2455, Riyadh 11451, Saudi Arabia

⁶ Department of Earth Sciences, Kanazawa University, Kanazawa 920-1192, Japan; aking826@staff.kanazawa-u.ac.jp

⁷ Geology Department, Faculty of Science, Zagazig University, Zagazig 44519, Egypt

* Correspondence: mohamed.khader1@sci.kfs.edu.eg or khedrzm75@gmail.com; Fax: +20-47-264-6545

Abstract: Beryl mineralization in the Nugrus-Sikait domain in the South Eastern Desert (SED) of Egypt occurs as disseminated crystals in granitic pegmatite and quartz, as well as pegmatite veins crosscutting mélange schist and ophiolitic rocks. When granitic pegmatite comes into contact with the ophiolitic rocks, phlogopite and amphibole schists are formed due to K metasomatism. The ophiolitic mélange is intruded by leucogranite and related pegmatite along the NNW to NW Nugrus shear zone. Beryl samples have been collected from Um Sleimat, Madinat Nugrus, Wadi Abu Rusheid, and Wadi Sikait. Major oxides and in situ trace and rare earth elements (REEs) of beryl and associated minerals were analyzed through EPMA and LA-ICP-MS, respectively. The investigated beryl, based on its color and chemical compositions, can be classified into the two following types: pegmatitic beryl (type I) and schist-related beryl (type II). The former is colorless to pale green, and is mainly restricted in pegmatite veins; it is poor in Cr₂O₃ (up to 0.03 wt%) and MgO (Nil). The latter, deep green in color, is rich in Cr₂O₃ (up to 0.27 wt%) and MgO (up to 2.71 wt%), and occurs within quartz veins, phlogopite schists, and tremolite schists. The abundant beryl mineralization in phlogopite schists and their related quartz veins suggests that granite and associated pegmatite are the source rocks for the Be-bearing fluids that migrate along the NW-SE trending deep-seated tectonic zone, such as the Nugrus shear zone. Therefore, the formation of beryl in schists is attributed to the interaction of granitic/pegmatitic-derived Be-bearing fluids with serpentinite and gabbro interlayered with mélange schists. Variations in the trace and REE contents of both beryl types (I and II) indicate their two-stage formation from different compositions of Be-rich fluids, where light REEs, Zr, Nb, Ba, and Th decrease from type I beryl to type II. These two phases of beryl could be attributed to the magmatic/hydrothermal fluids associated with the pegmatite emplacement. The early phase of the late-stage magmatic-derived fluids was closely related to magma evolution and pegmatite formation, forming euhedral type I beryl. The late phase of pegmatite-derived fluids was mixed with serpentinite/schist-derived fluids that cause high V and Cr content in type II beryl. The composition of parent magmas of felsic rocks, the high degree of magma fractionation or the late stage melts, fluid compositions (rich in Be, Li, Cs, Rb, K), and alkali metasomatism, as well as the linear NW-SE trending deep-seated shear zone, are all factors possibly influencing beryl mineralization in the SED of Egypt.



Citation: Khedr, M.Z.; Saleh, G.M.; Abdelfadil, K.M.; Takazawa, E.; Abdelrahman, K.; Tamura, A.; El-Shafei, S.A. The Geology and Mineral Chemistry of Beryl Mineralization, South Eastern Desert, Egypt: A Deeper Insight into Genesis and Distribution. *Minerals* **2024**, *14*, 465. <https://doi.org/10.3390/min14050465>

Academic Editor: Nikita V. Chukanov

Received: 18 March 2024

Revised: 24 April 2024

Accepted: 25 April 2024

Published: 28 April 2024



Copyright: © 2024 by the authors. Licensee MDPI, Basel, Switzerland. This article is an open access article distributed under the terms and conditions of the Creative Commons Attribution (CC BY) license (<https://creativecommons.org/licenses/by/4.0/>).

Keywords: beryl mineralization; pegmatite veins; phlogopite schist; in situ trace elements; mineral chemistry; Eastern Desert

1. Introduction

Beryl ($(K, Na, Cs, H_2O)(Al, Sc, Fe, Mg)_2(Be, Li)_3(Si_6 O_{18})$) is the main beryllium mineral, and is found mainly in felsic rocks [1]. It is the principal source of beryllium (Be) metal that is utilized in many versatile applications, such as alloys, telecommunications, nuclear reactors, space shuttles, vehicles, computers, and military equipment [1,2]; in alloys including copper or nickel, beryllium is used to create non-sparking tools, electrical contacts, gyroscopes, and spot-welding electrodes [2–7]. The ancient beryl mines in Egypt were found where the stream erosion exposed a concentration of emerald along the intrusive contact zone. Since the time of the Pharaohs, emerald (green beryl) and other colored varieties of beryl have been valued as rare gemstones in Egypt. Recently, beryl and its gem varieties have attracted the interest of many researchers due to their economic significance [2–7].

Beryl deposits from various geological settings worldwide can be classified into the following categories: (1) emerald-related schists; (2) beryl-bearing highly fractionated granite (S-type) and associated pegmatites; (3) hydrothermal beryl deposits related to metasomatized granite (e.g., greisen); (4) volcanogenic rock-hosted beryllium ore deposits; and (5) carbonate-hosted beryllium ore deposits [2,8]. High silica crustal granite and its related rocks, such as pegmatites and aplites, as well as quartz veins, are the most common sources of Be [3,9,10]. The beryllium (Be) concentration in such felsic rocks can reach up to 200 ppm [3,8], and is commonly associated with other lithophile metals, such as W, Sn, Mo, U, Nb, Ta, Th, and Li. The Be-bearing granitoids in Egypt can be distinguished into three types as follows [11,12]: (i) metasomatized Be-rich granite; (ii) Be-rich, Li-albite granite; and (iii) emerald associated with muscovite leucogranite. For the first and second types, Be mineralization is spatially and genetically related to post-orogenic granitoids, while, for the third category, beryl mineralization is closely related to the post-orogenic muscovite leucogranite and pegmatite in their contact aureoles.

The beryl deposits in Precambrian rocks in Egypt are divided into the following categories: (1) emerald in mica schists and (2) beryl in granitoid rocks and associated pegmatites [2]. Emerald is the green to pale green gem variety and the most common type of beryl. Its green color is attributed to the presence of trace amounts of Cr^{3+} and V^{3+} [13]. Mafic-ultramafic rocks and black shale are the main source of Cr and V in green emerald [3,14]. Emerald and other beryl deposits in Egypt are restricted in the South Eastern Desert (SED) and in south Sinai. The beryl mineralization in the SED occurs in the two small following belts: the Homret Akarem-Homret Mikpid (HA-HM) district and Zabara- Um Kabu (Z-UK) district [7,15,16]. These two belts are related to the Pan-African event, which involves a period of strong thermal activity and magmatism [17,18]. Beryl in the HA-HM district occurs as pockets, lenses, and disseminated crystals in alkali-feldspar granite, greisen, and albitized granite, as well as zones between quartz veins and metasediment [19]. The genesis of this beryl mineralization is interpreted as a result of metasomatism by the emanation of volatiles exsolved from a deep-seated highly evolved felsic magma source [20].

The spatial distribution of beryl mineralization in Z-UK is restricted in a defined zone with a NW-SE trend (Najd fault system), which is characterized by anomalous radioactivity, intense metamorphism, metasomatism, and mineralization, caused by acidic intrusions [16]. This extensive district coincides with the major Nugrus shear zone, which is linked to the Najd strike-slip shear-zone (NW-SE) system. The beryl mineralization in the Z-UK district occurs as disseminated crystals in quartz veins, pegmatites, and phlogopite schists [3,6,7,9,10]. This beryl occurrence reflects how the genesis of beryl mineralization in the Z-UK district is related to interactions between highly evolved felsic magma (of muscovite leucogranite and associated pegmatites) and the pre-existing mafic-ultramafic

rocks embedded in a *mélange* matrix (e.g., schist). This melt–rock interaction involves the addition of some elements (Be, F, B, P, alkalis), which characterize a highly evolved granitic assemblage, to the ultramafic assemblage, which is quite high in Mg, Ti, Cr, Ni, and Cu. Consequently, phlogopite (K-metasomatism) was formed at the expense of earlier actinolite (Mg, Ca metasomatism), which released Cr and/or V, thus providing the green to deep green color of beryl [3,6,7,9,10].

The coexistence of Be with other incompatible elements (Li, Rb, Cs, Sr, B, K) and the genesis of beryl in the SED of Egypt are important subjects, and are still the matter of debate. The current study discusses the geology and mineral chemistry (major and in situ traces and REEs) of beryl and associated mineral assemblages in order to understand the genesis and elucidate distribution of beryl mineralization in the SED of Egypt. It is the first time in situ traces and REEs of beryl in Egypt have been determined using LA-ICP-MS, which provides more accurate and precise data for the evaluation of the geochemical features of beryl mineralization. Four localities from the Z-UK district in the SED have been selected for the present study, including Wadi Sikait, Wadi Abu Rusheid, Madinat Nugrus, and Um Sleimat. This study also provides evidence for the role of the Najd shear zone in beryl mineralization in the Eastern Desert of Egypt.

2. Geologic Setting

The Zabara- Um Kabu (Z-UK) belt in the SED of Egypt (Figure 1a), which is part of the Arabian Nubian Shield (ANS), extends in a NW-SE (Najd fault trend) direction (45 km long and 10 km wide), relating to the Nugrus shear zone [3,6,7,9,10]. It is located 70 km southwest of the Marsa Alam city, and is delineated by latitudes of 24° 47' 00'' to 24° 34' 16'' N and longitudes of 34° 40' 00'' N to 34° 55' 00'' E. The emerald-bearing schists and rare metal-bearing rocks in the SED of Egypt are confined to this NW-SE linear belt [21]. The Z-UK district comprises three geologic areas as follows: Zabara, Nugrus-Sikait, and Um Kabu-Um Addebaa. The Nugrus-Sikait domain (the study area) is located at the central part of the Z-UK belt, and includes, from North to South, Wadi Sikait, Wadi Abu Rusheid, Wadi Nugrus, and Wadi El Gemal (Figure 1b). The area looks like a lenticular-shaped body with a wider NW end and a narrow SE end [21]. This linear distribution of beryl mineralization (Figure 1b) in the investigated region arranges along the NW-SE trend, where the distribution of the emerald mines occur. This beryl mineralization is possibly attributed to the effect of the NW-SE shear zone (Figure 1b). The rock units exposed in the Z-UK district include, from the oldest to youngest, the following: dismembered ophiolitic rocks (e.g., serpentinite, talc carbonate, and metagabbro), volcanogenic metasediment such as schists (forming a *mélange* matrix), granitic gneiss (orthogneiss), biotite granite, alkali-feldspar granite, and muscovite leucogranite with related pegmatites (Figure 1b). The district is dissected by post-orogenic pegmatite veins, quartz veins, and lamprophyre dykes [22] (Figure 1b). The ophiolitic rocks and associated metasediments were intruded by mica granite and related pegmatites along their contacts, forming mineralized zones enriched with beryl and rare metals [2].

The dismembered ophiolite in the Nugrus-Sikait area is mainly represented by ultramafic rocks (serpentinite and talc-carbonate) and ophiolitic metagabbro. The ophiolitic *mélange* is composed of fragments and blocks of ultramafic rocks, tectonically embedded in a fine- to coarse-grained matrix. The *mélange* matrix is mainly schistose rocks that include boudinage pegmatites, extending parallel to the foliation planes. These schistose rocks in Wadi Sikait comprise talc schists, graphite schists, mica schists, garnet-mica schists, and quartzo-feldspathic schists. The beryl mineralization is mainly hosted by mica schists, besides elongate crystals disseminated in amphibole schists [23].

The ophiolitic *mélange* is thrust over orthogneiss by a low-angle thrust fault (Nugrus ductile shear zone), trending NW-SE and dipping 30° SW. The age of thrusting plausibly falls between 682 Ma (the time of emplacement of the older granitoid) and 600 Ma, which is the upper time limit of the granite intrusion [24]. Recently, this NW-SE thrust fault, which is related to the Najd fault system, yielded 620–540 Ma [25], and this is possibly the time

of beryl mineralization. The thrust contact between gneiss and overthrust ophiolitic mélangé rocks is characterized by strong deformation, forming several folds in serpentinite in the ophiolitic mélangé. It acts as a zone of weakness or a pathway for the intruded felsic magma (leucogranite and related pegmatite) and magma-derived fluids. The granitic pluton elongated in the NW-SE direction (12 km in length) and thinned in the NE-SW direction (3 km in width), forming a nearly spherical-like shape with cataclastic rocks at its core [26]. The granitic rocks are represented by porphyritic biotite granite, alkali-feldspar granite, and muscovite leucogranite, which occurs as small masses in Um Sleimat, W. Sikait, and Abu Rusheid. This leucogranite (sometimes acting as the host of beryl-rich veins) exists as offshoots, emplacing into the ophiolitic mélangé and metagabbro in Madinat Nugrus and Um Sleimat. It also occurs as dike-like injected bodies, emplacing into porphyritic biotite granite in W. Sikait.

The ophiolitic rocks and orthogneiss underwent progressive metamorphism and deformation along the NW-SE shear zone. The serpentinite was transformed into talc-carbonate, while the metagabbro is thrust over the ophiolitic mélangé, forming a sheeted mass [23]. The deformed orthogneiss is represented by mylonite, and contains blocks of mafic-ultramafic rocks and bands of tremolite–actinolite. The mylonitic rocks are highly foliated, and include pegmatitic and quartz veins (host of beryl), which are parallel to the foliation planes. These rocks are highly tectonized and foliated with minor to major folds. They are cut by two shear zones, showing NW-SE and NE-SW trends [22].

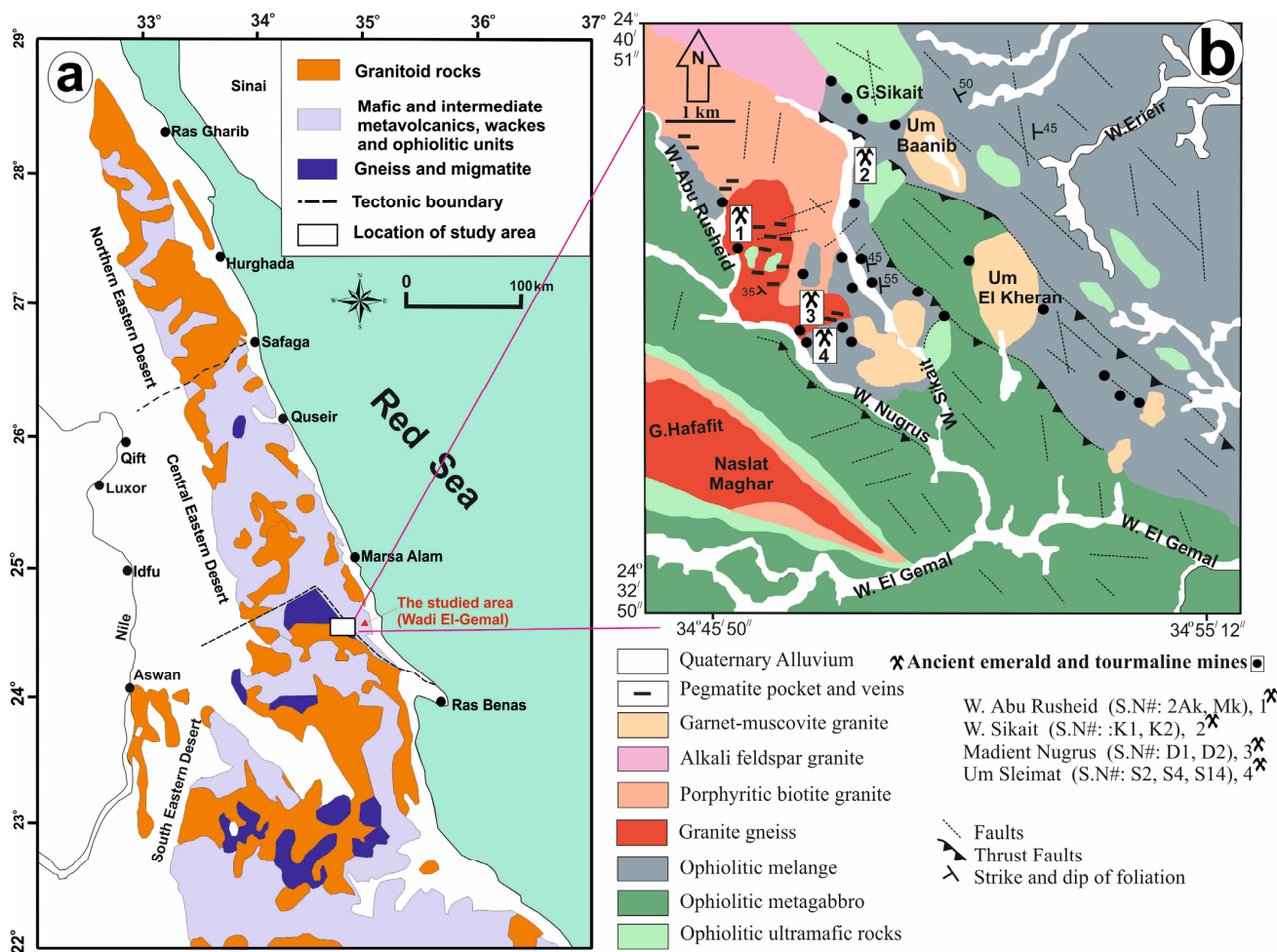


Figure 1. (a) Geological map of the Eastern Desert of Egypt, showing the distribution of basement rocks and the study areas (Modified after Stern and Ali [27]). **(b)** Geological map of the Nugrus-Sikait area in the SED of Egypt, including four locations of beryl: (1) Wadi Abu Rusheid, (2) Wadi Sikait, (3) Madinat Nugrus, and (4) Um Sleimat.

3. Sample Description and Beryl Mineralization

The beryl deposits in the Z-UK district were mined from Wadi Sikait, the oldest emerald mine in the world, in addition to several other sites within a 15 km radius of Wadi Sikait, including Gebel Zabara, Wadi Nugrus and Um Sleimat, Wadi Abu Rusheid, Wadi Umm Kabu, Wadi Um Addebaa, and Wadi El Gemal (Figure 1b). More than 200 ancient tunnels for emerald mining are recorded along Z-UK [7,28]. Some of these mining activities began in Pharaonic times, and continued into the Roman and Byzantine periods [19]. Beryl samples for this study were collected from four areas in the Z-UK district, including Um Sleimat, Wadi Nugrus (Madinat Nugrus), Wadi Abu Rusheid, and Wadi Sikait (Figure 1b). The beryl mineralization in the Z-UK district is confined to the contact between orthogneiss (granite gneiss) and the overthrust ophiolitic mélangé rocks along the major Nugrus shear zone (NW-SE) and related structures [11,28]. However, Khaleal et al. [6] stated that, in the Z-UK district, the beryl mineralization occurs at the intrusive contact between the ophiolitic mélangé rocks and the intruding felsic magma of muscovite leucogranite and related pegmatite.

There are ancient beryl mining sites in Wadi Um Sleimat (Figure 1b), with trends of N-S and NNW-SSE. Um Sleimat beryl mineralization is found in phlogopite schists, tourmaline schists, and in quartz veins at the intrusive contact between the ophiolitic mélangé and muscovite granites (Figure 2a,b). Phlogopite zones around beryl-bearing quartz veins extend in the NW-SE direction, and dip 35°–65° to the NE [7,23,28]. The unmineralized quartz veins (beryl-free veins) are not surrounded by phlogopite schists and/or cut the ultramafic rocks. In addition, some pegmatite veins in Um Sleimat intrude metagabbro in some places.

Beryl mining sites in the Wadi Sikait-Nugrus domain show striking NW-SE and NNW-SSE trends. The beryl mineralization occurs as disseminated crystals, either in phlogopite schists and its related quartz veins (Figure 2c,d) or in pegmatite veins related to muscovite leucogranite (Figure 2e,f). The occurrence of beryl is intimately linked with the Be-enriched milky quartz [3,29]. The beryl deposits in this domain mainly occur as vein-type deposits at the intrusive contact between ophiolitic ultramafic rocks and the granite intrusions [30,31] (Figure 2c,d), and/or occur along the contact zone between biotite schists, pegmatites, and quartz veins [2]. All these beryl-bearing rocks are confined to the Nugrus ductile shear zone, trending in the NW-SE direction. The pegmatite/quartz veins intruded all older rock units in the Nugrus-Sikait domain; they vary from few centimeters up to one meter in thickness, and usually host Be, Th, U, Li, and Nb-Ta mineralization. Beryl in phlogopite schists is almost monomineralic, consisting essentially of coarse phlogopite flakes (Figure 2c,d), and is characterized by a silky sheen surface in hand specimens.

Several old beryl mines are observed in Wadi Abu Rusheid, where mineralization follows a NNW-SSE trend. Abu Rusheid beryl deposits occur at the contact between the ophiolitic mélangé and both orthogneiss (granitic gneiss) and biotite granites. They are mainly found as disseminated crystals in pegmatite-related quartz veins, pegmatite veins (Figure 2g,h), and granitic pegmatite, but are rarely found in phlogopite schists.

In summary, beryl shows variations in color, from colorless, pale green to deep transparent green, and is mainly embedded in white milky quartz, especially when in contact with phlogopite schist. Beryl also varies in size and occurs as individual crystals (up to 4 cm in length) and/or aggregates either in phlogopite schists (Figure 2a,b) or in pegmatite/quartz veins (Figure 2e–h). In addition, coarse hexagonal prismatic beryl grains in pegmatite veins occur as euhedral crystals and are homogenous in color with high relief, but beryl crystals in quartz veins are corroded or dissected by quartz strings.

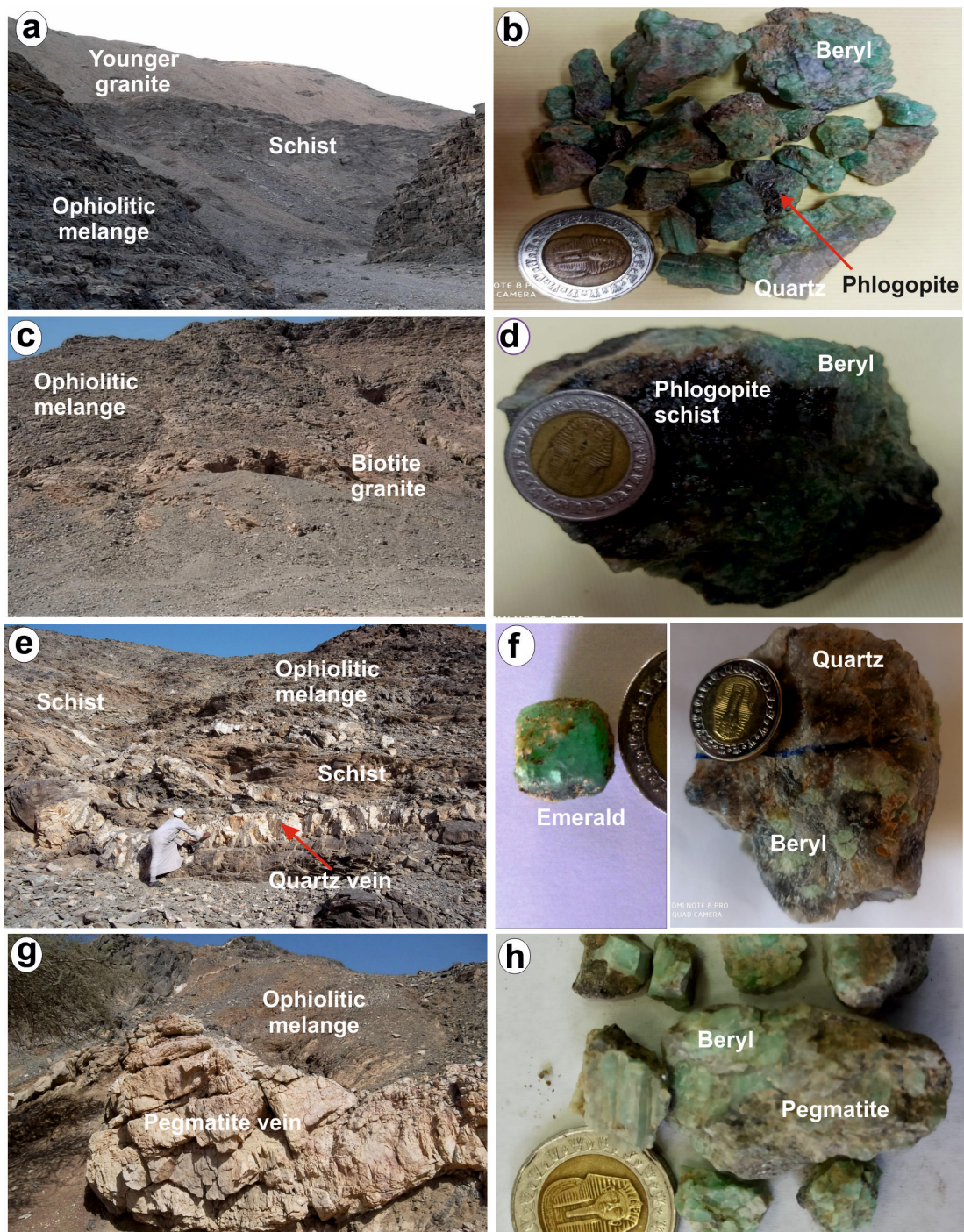


Figure 2. Field photographs of beryl mineralization in basement rocks from the Nugrus-Sikait domain, in the SED of Egypt. (a) Post-orogenic granite (younger granite, 550–640 Ma) intruded in the foliated ophiolitic mélangé, including the mine dump and old beryl mines in Wadi Um Sleimat. (b) Hand specimen of anhedral beryl crystals hosted by quartz veins and phlogopite schists, belonging to the ophiolitic mélangé in Wadi Um Sleimat. (c) The ancient tunnels and dumps of beryl at the contact between the ophiolitic mélangé and biotite granites in Wadi Sikait. (d) Hand specimen of beryl-bearing phlogopite schists belonging to the ophiolitic mélangé, Wadi Sikait. (e) Beryl-bearing quartz veins cutting in the ophiolitic mélangé (e.g., volcanogenic metasediments), Madinat Nugrus. (f) Hand specimen of euhedral olive-green beryl and pale green beryl in Madinat Nugrus. (g) Beryl-bearing pegmatite veins cutting the ophiolitic mélangé in Wadi Abu Rusheid. (h) Hand specimen of pale green anhedral to euhedral beryl crystals in Wadi Abu Rusheid.

4. Methodology

The major element contents of phlogopite (14 points) with the number of oxygen per formula (n.O.p.f, 22) within quartz and pegmatite veins hosted by granites and schists are as follows: biotite (9 points; n.O.p.f, 22), muscovite (4 points; n.O.p.f, 22), beryl (35 points; n.O.p.f, 18), plagioclase (4 points; n.O.p.f, 8), amphibole (6 points; n.O.p.f, 23), rutile (5 points; n.O.p.f, 2), chlorite (1 point; n.O.p.f, 28), orthopyroxene (1 point; n.O.p.f, 6), and titanite (1 point; n.O.p.f, 5) (Supplementary Table S1a). These values were determined using an electron probe microanalyzer (EPMA) with wavelength dispersive X-ray spectrometry (JEOL JXA-8600SX, JEOL Ltd., Tokyo, Japan), all housed at Niigata University, Japan. The operating conditions were 15 kV accelerating voltage, 13 nA beam current, and ~1 mm beam diameter. The data were corrected through the use of oxide ZAF matrix correction. Calibrations were performed using natural and synthetic standards at Niigata University; these standards were wollastonite for SiO₂ and CaO, corundum for Al₂O₃, olivine for Mg, Jadeite for Na₂O, eskolaite for Cr₂O₃, hematite for FeO, MnOFe₂O₃ for MnO, nickel oxide for NiO, rutile for TiO₂, KTiOPO₄ for K₂O, and SrBaNb₄ for BaO. The measurements of Si, Al, Mg, and Na were determined using channel 1 TAP, but Cr, Fe, Mn, and Ni were measured using channel 2 LIF. In addition, Ti, Ca, K, and Ba were determined using channel 3 PET. Beryl and associated mica were carried out using scanning electron microscopy (SEM)–energy dispersive X-ray spectroscopy (EDS) at Niigata University, Japan. The operating conditions included a 20 kV accelerating voltage and a working distance (WD) of 10 mm. To estimate the H₂O in beryl at Niigata University, the coarse beryl crystals have been picked from crushed granitic pegmatite and quartz. These crystals were ground up to 63 microns, forming beryl powders. The experimental measurement H₂O values were estimated via gradually heating beryl powders to 1000 °C (for 12 h) and determining the weight loss before and after heating a definite amount of the powder. The BeO was calculated after adding these H₂O values to other EPMA components of beryl (Table 1) and assuming a total of 100 wt%. Then, BeO wt% was estimated at 100% minus the sums of other EPMA beryl components.

The trace-element concentrations of beryl (32 points), phlogopite (3 points), and muscovite (1 point) (Supplementary Table S1b) within quartz and pegmatite veins hosted by granites and schists were determined in situ using laser-ablation (193 nm ArF excimer: MicroLas GeoLas Q-plus)–inductively coupled plasma mass spectrometry (LA-ICP-MS) at Kanazawa University, Japan. Analyses were achieved through the use of ablating 60 µm diameter spots. All analyses were carried out at 6 Hz with an energy density of 8 J/cm² per pulse. The total time of the data acquisition for one spot was 105 s, including laser ablation for 45 s and the analysis of the background before and after, for 40 s each. NIST 612 glass [32] was used as an external standard for the calibration of trace element concentrations, and ²⁹Si was used as an internal standard for all silicates based on the SiO₂ concentration obtained using electron microprobes. The precision or reproducibility is better than 4% for most elements, except Sc, Cr, and Ni, for which it is better than 12%. The accuracy and data quality were calculated based on reference material NIST 614.

5. Petrography

Representative samples of beryl-bearing quartz and granitic pegmatite lenses/veins, as well as their host mélange schist and granite in the study area, were selected for the petrographic study. The mélange matrix generally consists of phlogopite schists, amphibole schists, and biotite schists. Quartz lenses are essentially formed from quartz (55–65 vol.%) and beryl (30–40 vol.%), together with phlogopite (Figures 3 and 4). The beryl occurs as euhedral to subhedral crystals with high relief, homogenous in color (Figures 3a,b and 4a,b), and ranges in size from medium (<1 mm in diameter) to coarse (>1 mm in diameter) grains. Typical six-sided euhedral beryl is also observed in some quartz parts in pegmatite, showing a distinct triple junction boundary with serrated quartz (Figure 3a,b). In some quartz veins, beryl exists as coarse fractured crystals with open spaces partially filled with phlogopite (Figure 3c) or quartz strings (Figure 4a,b). Cracked beryl crystals corroded by quartz

(Figure 4a,b) are also recorded in some samples. Beryl is generally homogenous in color under polarized light or scanning electron microscopy (SEM) images (Figure 4a,b). Quartz occurs either as undulatory megacrysts (Figure 3a) or as medium interlocked crystals with serrated boundaries around the euhedral beryl crystals (Figure 3d). The investigated granitic pegmatite is mainly composed of plagioclase (30–40 vol.%), quartz (20–25 vol.%), K-feldspar (10–20 vol.%), and beryl (8–20 vol.%), together with muscovite, deformed phlogopite, and apatite (Figures 3e,f and 4a–e). Beryl is also found in the form of aggregated euhedral megacrysts sieved with fine muscovite and phlogopite blebs (Figure 3d,e). The granitic pegmatites found as elongated masses along the NW–SE Nugrus belt are composed of megacrysts of plagioclase, quartz, and K-feldspar, with subordinate muscovite, biotite, garnet, chlorite, zircon, apatite, euhedral beryl, and other rare metals.

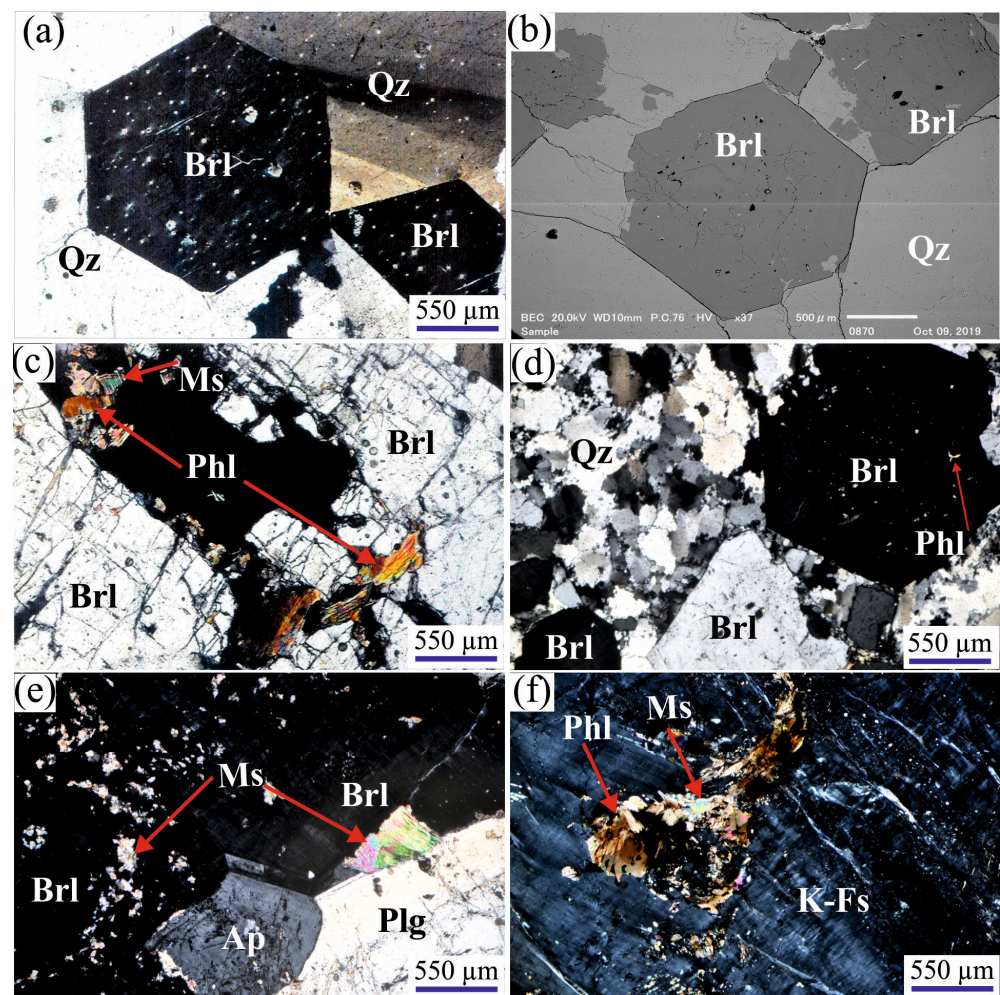


Figure 3. Photomicrographs in cross-polarized light of the studied pegmatites, except (b) is a scanning electron microscope (SEM) image. (a) Clear hexagonal euhedral beryl (Brl) crystal in a matrix of quartz (Qz) megacrysts; Abu Rusheid quartz vein. (b) Homogenous six-sided euhedral beryl (emerald) crystals in a matrix of interlocked quartz grains. (c) Coarse columnar beryl crystal including interstitial phlogopite (Phl) and muscovite (Ms) flakes, and invaded by quartz veinlets; Sikait quartz vein. (d) Inclusions of fine phlogopite blebs or fibers within coarse emerald crystal embedded in serrated quartz; Madinat Nugrus phlogopite schist. (e) Fine muscovite blebs and interstitial subhedral flake of muscovite-corroding homogeneous megacrysts of euhedral beryl, forming sharp contact with apatite (Ap) and plagioclase (Plg); Abu Rusheid pegmatite. (f) K-feldspar (K-Fs) megacrysts with perthitic texture, including phlogopite (Phl) and muscovite (Ms) flakes; Abu Rusheid pegmatite.

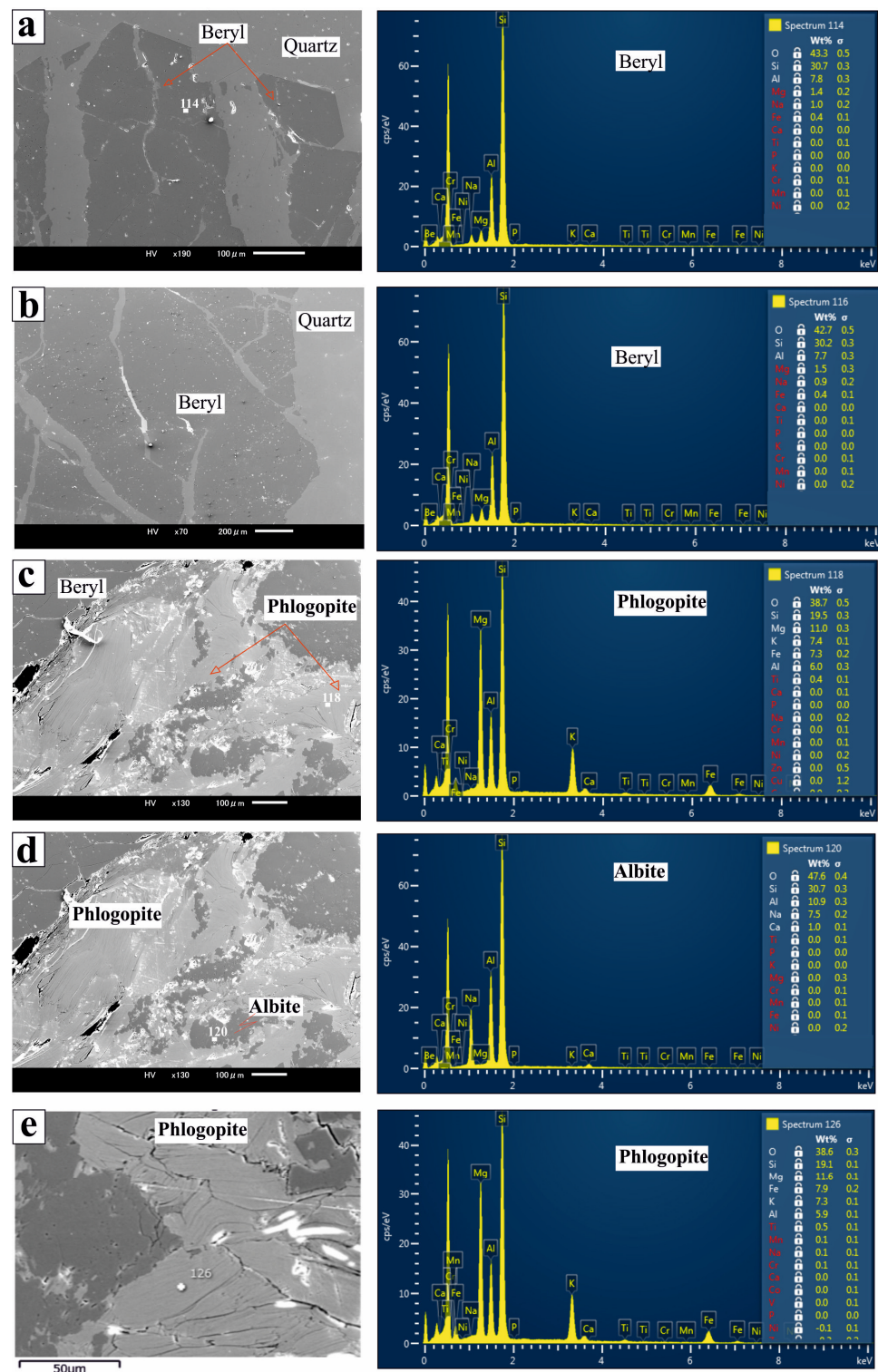


Figure 4. Scanning electron microscopy (SEM) images with the EDS spectrum analysis of beryl and associated phlogopite, quartz, and albite in pegmatite and quartz veins. (a) Subhedral beryl crystals dissected by quartz veins, showing homogenous composition without zonation. (b) Coarse subhedral beryl crystal veined with quartz string. (c,d) Anhedral to subhedral phlogopite plates with altered rims (secondary origin), showing a sharp boundary with subhedral beryl crystals in quartz and an albite matrix of pegmatite veins. (e) Deformed phlogopite flake (secondary origin) with clear bending due to deformation in beryl-bearing quartz veins.

The studied phlogopite schist is mainly composed of phlogopite and beryl together with minor chlorite and quartz. Beryl occurs as coarse hexagonal prismatic crystals (euhedral, early phase) wrapped by phlogopite; it is also found as fractured or tectonized crystals (subhedral, late phase) with open spaces partially filled with phlogopite (Figure 4c–e). Phlogopite frequently exists as flakes within coarse beryl crystals (Figure 4c–e). The amphibole schist comprises tremolite–actinolite, plagioclase, beryl, and titanite. The biotite schist is mainly composed of biotite and plagioclase together with rutile and minor quartz. Mylonite rocks are also observed along the NNW–SSE Nugrus shear zone, showing mylonitic fabric due to Nugrus ductile and brittle deformations. They comprise quartz, feldspar, and mica, such as muscovite and biotite, with subordinate chlorite and rare metals.

6. Results

6.1. Mineral Chemistry

6.1.1. Major Oxides

Representative microprobe analyses of the investigated beryl and mica are provided in Tables 1 and 2, respectively. The chemical analyses of gangue minerals such as amphibole, plagioclase, quartz, rutile, titanite, and chlorite are listed in Supplementary Table S1a.

The studied beryl is essentially composed of SiO_2 (63.0–67.13 wt%) and Al_2O_3 (12.68–17.89 wt%) (Table 1). The BeO (12.1–14.76 wt%) content of the analyzed beryl was calculated based on the standard formula of beryl (e.g., [33]) after experimentally measuring the H_2O values (1.2–2.5 wt%) and assuming a total of 100 wt%. The beryl in the Abu Rusheid pegmatite and pegmatitic quartz vein was depleted in Cr_2O_3 (0.0–0.03 wt%), MgO (0.0–0.01 wt%), and Na_2O (0.18–0.42 wt%), but was enriched in Al_2O_3 (16.68–17.89 wt%) relative to beryl in other areas, i.e., Cr_2O_3 : 0.01–0.27 wt%, MgO: 2.12–2.71 wt%, Na_2O : 0.84–1.84 wt%, and Al_2O_3 : 14.14–15.36 wt%. The subordinate content of Cr_2O_3 (up to 0.27 wt%) provides the green color chromophore of beryl crystals in Um Sleimat, Sikait, and Madinat Nugrus. Other major oxides such CaO (up to 0.05 wt%), K_2O (up to 0.08 wt%), TiO_2 (up to 0.06 wt%), and MnO (up to 0.05 wt%) are low in concentration. The average contents of BeO (13.2 wt%), FeO^t , Cr_2O_3 , and MgO in the studied beryl are similar to contents of most emerald minerals in Africa [34,35].

The Al_2O_3 of Um Sleimat beryl in quartz veins is negatively correlated with all MgO, FeO, and Na_2O (Figure 5a–c), suggesting the partial ionic substitution of octahedral Al by Mg and Na. In Sikait beryl, the Al_2O_3 shows a strong negative correlation with both MgO and FeO (Figure 5d,e), but a weak positive correlation with Na_2O (Figure 5f). Moreover, in Madinat Nugrus, the Al_2O_3 exhibits a strong negative correlation with MgO (Figure 5g), and a weak correlation with both FeO and Na_2O (Figure 5h,i). In addition, Al_2O_3 of Abu Rusheid beryl is strongly correlated with FeO (Figure 5k), but weakly correlated with both Na_2O and MgO (Figure 5j,l).

Table 1. Representative EMPA of beryl in the study area.

Location	Madinat Nugrus							Um Sleimat			Sikait			Abu Rusheid					
Rock Type	Phlogopite Schist				Quartz Vein			QUARTZ VEIN			Quartz Vein		Tremolite Sch.		Pegmatite Vein				
Sample No.	D1		D2			S2			K1		K2		1MK						
Spot No.	224	226	231	258	263	265	288	283	278	239	234	236	238	9	12	241	245	246	247
SiO ₂	66.24	66.24	66.13	65.16	65.68	65.23	65.78	66.62	66.81	65.093	65.72	64.51	65.78	66.00	65.23	64.75	65.27	66.03	65.025
TiO ₂	0.057	0	0	0	0.004	0	0.032	0	0	0	0	0	0.023	0.00	0.00	0	0	0.028	0
Al ₂ O ₃	14.73	15.13	14.47	14.94	14.17	14.83	15.01	14.545	15.113	15.047	14.6	14.72	14.56	12.68	13.32	17.78	16.72	17.89	16.676
Cr ₂ O ₃	0.021	0	0.043	0.074	0.266	0.062	0.035	0.014	0.013	0.126	0.089	0.059	0.208	0.57	0.44	0.014	0	0	0.034
FeO	0.553	0.558	0.432	0.574	0.609	0.516	0.548	0.767	0.771	0.425	0.59	0.465	0.627	0.65	0.66	0.816	2.026	0.249	1.937
MnO	0.031	0.008	0.003	0.014	0	0.006	0.032	0.013	0	0.013	0.025	0.053	0.047	0.00	0.00	0	0.03	0	0.008
MgO	2.405	2.358	2.383	2.344	2.599	2.194	2.226	2.709	2.301	2.123	2.29	2.296	2.242	2.10	2.28	0.005	0.001	0	0.002
CaO	0.026	0.017	0.014	0.026	0.031	0.009	0.023	0.035	0.028	0.031	0.02	0.047	0.019	0.06	0.03	0	0.005	0	0.001
Na ₂ O	0.838	1.019	1.062	1.051	1.397	1.33	1.595	1.842	1.521	1.214	1.11	1.215	1.313	2.35	2.12	0.177	0.212	0.418	0.242
K ₂ O	0.032	0.019	0.025	0.054	0.08	0.025	0.031	0.07	0.042	0.022	0.023	0.031	0.006	0.03	0.02	0	0.015	0.002	0.024
NiO	0.014	0	0	0.006	0	0	0	0.014	0	0.025	0	0	0.061	0	0	0	0	0	0
BaO	0.025	0.068	0	0.047	0.026	0	0	0	0	0.035	0	0.011	0	0	0	0	0	0.018	0
Total	84.97	85.41	84.56	84.24	84.88	84.23	85.31	86.63	86.60	84.15	84.47	83.40	84.89	84.44	84.11	83.55	84.28	84.63	83.95
BeO*	12.63	12.19	13.04	13.96	13.32	13.97	13.47	12.15	12.18	13.36	13.04	14.11	12.63	13.10	13.43	13.96	13.22	12.87	13.55
H ₂ O*	2.4	2.4	2.4	1.8	1.8	1.8	1.22	1.22	1.22	2.49	2.49	2.49	2.49	2.46	2.46	2.5	2.5	2.5	2.5
Si	5.91	5.92	5.89	5.77	5.84	5.77	5.81	5.92	5.92	5.81	5.86	5.75	5.89	5.92	5.85	5.73	5.82	5.85	5.79
Ti	0.004	0.000	0.000	0.000	0.000	0.000	0.002	0.000	0.000	0.000	0.000	0.000	0.002	0.000	0.000	0.000	0.000	0.002	0.000
Al	1.547	1.592	1.518	1.558	1.483	1.547	1.561	1.522	1.578	1.582	1.535	1.545	1.536	1.341	1.407	1.855	1.758	1.867	1.751
Cr	0.001	0.000	0.003	0.005	0.019	0.004	0.002	0.001	0.001	0.009	0.006	0.004	0.015	0.041	0.032	0.001	0.000	0.000	0.002
Fe	0.041	0.042	0.032	0.042	0.045	0.038	0.040	0.057	0.057	0.032	0.044	0.035	0.047	0.049	0.049	0.060	0.151	0.018	0.144
Mn	0.002	0.000	0.000	0.001	0.000	0.000	0.002	0.001	0.000	0.001	0.001	0.003	0.003	0.000	0.000	0.000	0.002	0.000	0.000
Mg	0.320	0.314	0.316	0.309	0.344	0.290	0.293	0.359	0.304	0.282	0.305	0.305	0.299	0.281	0.305	0.001	0.000	0.000	0.000
Ca	0.002	0.002	0.001	0.002	0.003	0.001	0.002	0.003	0.003	0.003	0.002	0.004	0.002	0.006	0.003	0.000	0.000	0.000	0.000
Na	0.145	0.176	0.183	0.180	0.241	0.228	0.273	0.317	0.261	0.210	0.192	0.210	0.228	0.408	0.369	0.030	0.037	0.072	0.042
K	0.004	0.002	0.003	0.006	0.009	0.003	0.003	0.008	0.005	0.003	0.003	0.004	0.001	0.003	0.003	0.000	0.002	0.000	0.003
Ni	0.001	0.000	0.000	0.000	0.000	0.000	0.000	0.001	0.000	0.002	0.000	0.000	0.004	0.000	0.000	0.000	0.000	0.000	0.000
Ba	0.001	0.002	0.000	0.000	0.002	0.001	0.000	0.000	0.000	0.001	0.000	0.000	0.000	0.000	0.000	0.000	0.000	0.001	0.000
Be	2.704	2.614	2.788	2.967	2.844	2.971	2.856	2.591	2.592	2.861	2.795	3.018	2.714	2.824	2.891	2.967	2.832	2.738	2.900
Total	10.67	10.66	10.73	10.83	10.82	10.85	10.84	10.77	10.71	10.79	10.74	10.87	10.73	10.87	10.90	10.64	10.60	10.54	10.63

BeO* was calculated after adding the H₂O values to the EPMA data and assuming a total of 100 wt%. H₂O* was experimentally estimated by determining the weight loss of beryl powders.

Table 2. Representative EMPA (wt%) of mica associated with beryl.

Location	Um Sleimat				Madinat Nugrus				Abu Rusheid				Sikait						
Rock Type	Quartz Vein				Phlogopite Schist				Pegmatite Vein				Biotite Schist						
Mineral Type	Phlogopite				Muscovite				Biotite										
Sample No.	S2		S4		S14		D1		D3		1MK		T50						
Spot No.	285	286	14	21	22	225	230	3	6	243	248	15	35	37	38	41	42	44	45
SiO ₂	43.12	43.72	47.10	46.96	49.15	41.30	41.30	49.00	46.54	51.15	50.35	47.24	39.44	38.57	40.02	39.36	39.15	39.47	39.36
TiO ₂	0.78	0.73	0.71	0.92	0.91	0.99	0.99	0.68	0.67	0.09	0.10	0.09	1.63	1.83	1.70	1.61	1.55	1.23	1.15
Al ₂ O ₃	13.24	13.42	12.54	12.93	11.96	14.67	14.67	10.70	11.29	30.60	28.60	29.25	18.11	18.10	18.93	18.07	18.19	18.59	18.35
Cr ₂ O ₃	0.00	0.05	0.05	0.10	0.08	0.00	0.00	0.12	0.11	0.00	0.00	--	0.00	0.01	0.02	0.00	0.00	0.03	0.05
FeO	10.48	9.91	9.09	8.60	7.53	9.64	9.64	8.22	6.03	5.85	7.60	7.57	9.08	9.45	9.51	8.84	9.00	9.34	8.90
MnO	0.14	0.05	0.13	0.11	0.11	0.03	0.03	0.08	0.06	0.01	0.00	0.90	0.08	0.06	0.08	0.08	0.12	0.09	0.04
MgO	20.07	19.74	19.73	16.57	15.94	20.65	20.65	15.63	20.15	0.05	0.06	0.04	17.60	18.24	18.45	18.23	18.60	18.65	19.27
CaO	0.00	0.01	0.18	0.18	0.18	0.04	0.04	0.29	0.09	0.00	0.00	0.13	0.03	0.01	0.05	0.01	0.01	0.02	0.10
Na ₂ O	0.32	0.42	0.39	0.76	0.81	0.20	0.20	1.03	0.65	0.04	0.03	0.45	0.46	0.50	0.50	0.42	0.56	0.44	0.55
K ₂ O	9.35	8.91	6.52	8.28	8.35	9.24	9.24	9.83	11.02	10.33	9.98	9.83	8.92	8.91	8.80	9.29	8.89	9.34	8.63
BaO	0.09	0.06	0.17	0.14	0.12	0.20	0.20	0.13	0.10	0.00	0.01	--	0.20	0.18	0.22	0.24	0.14	0.14	0.22
NiO	0.02	0.04	--	--	--	0.00	0.00	--	--	0.00	0.00	--	0.03	0.00	0.03	0.05	0.05	0.08	0.08
Total	97.62	97.04	96.61	96.53	96.10	96.97	96.97	96.69	96.71	98.11	96.73	95.50	95.57	95.85	98.32	96.20	96.25	97.40	96.68
Si	6.08	6.16	6.50	6.60	6.87	5.86	5.86	6.91	6.52	6.69	6.74	6.48	5.65	5.54	5.58	5.62	5.58	5.57	5.57
Al ^{iv}	1.92	1.84	1.50	1.40	1.13	2.14	2.14	1.09	1.48	1.31	1.26	1.52	2.35	2.46	2.42	2.38	2.42	2.43	2.43
Al ^{vi}	0.28	0.38	0.54	0.74	0.84	0.31	0.31	0.69	0.38	3.41	3.26	3.21	0.71	0.60	0.69	0.65	0.63	0.66	0.63
Ti	0.08	0.08	0.07	0.10	0.10	0.11	0.11	0.07	0.07	0.01	0.01	0.01	0.18	0.20	0.18	0.17	0.17	0.13	0.12
Cr	0.00	0.01	0.01	0.01	0.01	0.00	0.00	0.01	0.01	0.00	0.00	0.00	0.00	0.00	0.00	0.00	0.00	0.00	0.01
Fe	1.24	1.17	1.05	1.01	0.88	1.14	1.14	0.97	0.71	0.64	0.85	0.87	1.09	1.13	1.11	1.05	1.07	1.10	1.05
Mn	0.02	0.01	0.02	0.01	0.01	0.00	0.00	0.01	0.01	0.00	0.00	0.10	0.01	0.01	0.01	0.01	0.01	0.01	0.01
Mg	4.22	4.14	4.06	3.47	3.32	4.37	4.37	3.29	4.21	0.01	0.01	0.01	3.76	3.90	3.83	3.88	3.95	3.92	4.07
Ni	0.00	0.00	0.02	0.02	0.01	0.00	0.00	0.01	0.01	0.00	0.00	0.00	0.00	0.00	0.00	0.01	0.01	0.01	0.01
Ca	0.00	0.00	0.03	0.03	0.03	0.01	0.01	0.04	0.01	0.00	0.00	0.02	0.00	0.00	0.01	0.00	0.00	0.00	0.02
Na	0.09	0.11	0.10	0.21	0.22	0.06	0.06	0.28	0.18	0.01	0.01	0.12	0.13	0.14	0.14	0.12	0.16	0.12	0.15
K	1.68	1.60	1.15	1.48	1.49	1.67	1.67	1.77	1.97	1.72	1.70	1.72	1.63	1.63	1.56	1.69	1.61	1.68	1.56
Ba	0.01	0.00	--	--	--	0.01	0.01	--	--	0.00	0.00	--	0.01	0.01	0.01	0.01	0.01	0.01	0.01
OH*	4.00	4.00	4.00	4.00	4.00	4.00	4.00	4.00	4.00	4.00	4.00	4.00	4.00	4.00	4.00	4.00	4.00	4.00	4.00
Total	19.62	19.51	19.03	19.08	18.90	19.67	19.67	19.15	19.55	17.81	17.84	18.06	19.52	19.62	19.54	19.60	19.62	19.65	19.63
Fe/Fe+Mg	0.23	0.22	0.21	0.23	0.21	0.21	0.21	0.23	0.14	0.98	0.99	0.99	0.22	0.23	0.22	0.21	0.21	0.22	0.21
XFe	0.26	0.27	0.28	0.34	0.34	0.25	0.25	0.34	0.20	1.00	1.00	1.00	0.32	0.31	0.32	0.31	0.30	0.31	0.29
Mg/(Mg+Fe)	0.77	0.78	0.79	0.77	0.79	0.79	0.79	0.77	0.86	0.02	0.01	0.01	0.78	0.77	0.78	0.79	0.79	0.78	0.79
T °C	594	593	597	621	633	617	617	600	624				687	702	687	690	680	642	640
fO ₂	-20.7	-20.7	-20.6	-19.6	-19.2	-19.8	-19.8	-20.4	-19.5				-17.2	-16.7	-17.2	-17.1	-17.5	-18.8	-18.9

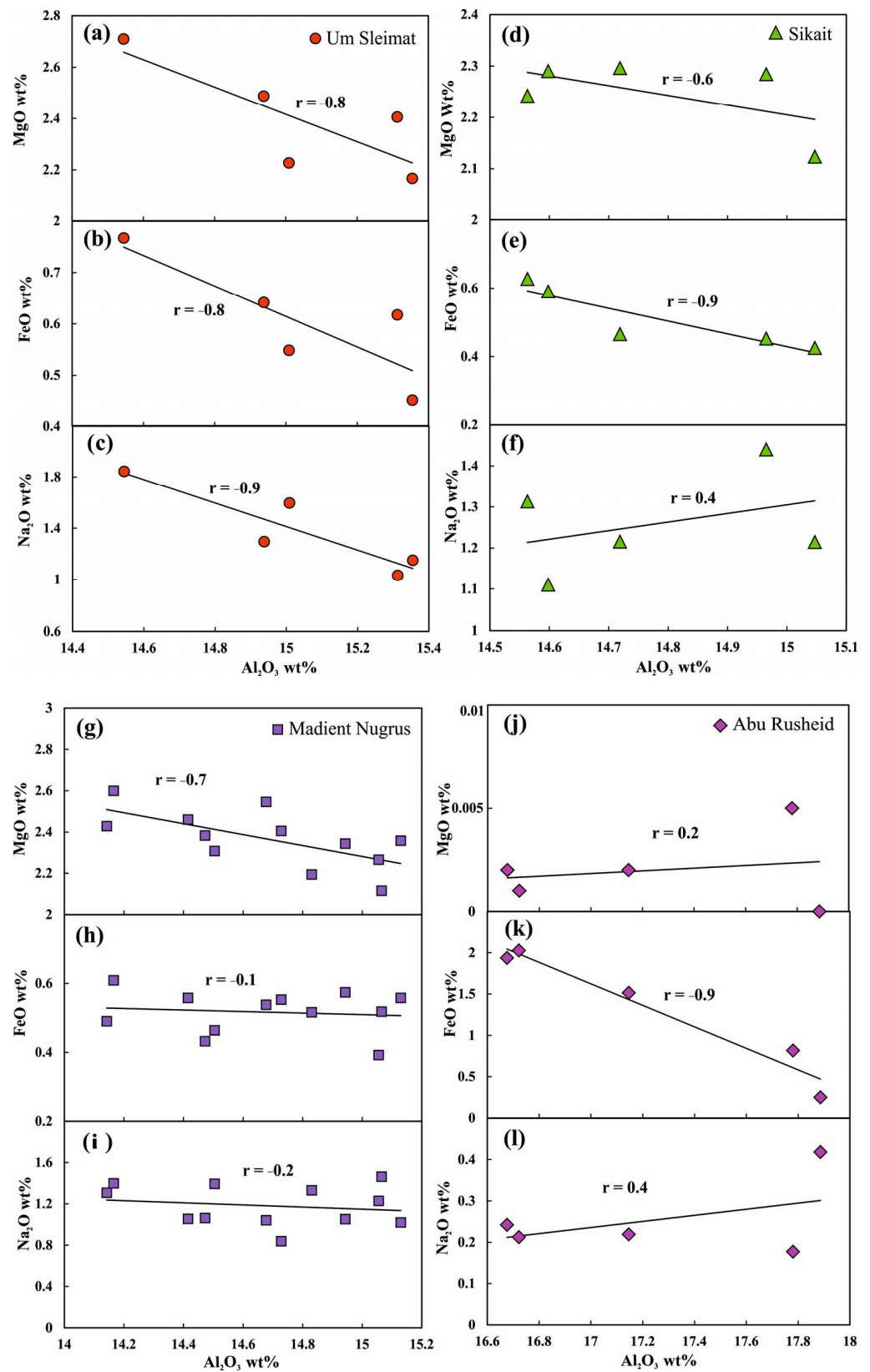


Figure 5. Substitution diagrams of beryl from granitic pegmatites. (a–c) Al_2O_3 vs. MgO, FeO, and Na_2O in Um Sleimat beryl. (d–f) Al_2O_3 vs. MgO, FeO, and Na_2O in Sikait beryl. (g–i) Al_2O_3 vs. MgO, FeO, and Na_2O in Madinat Nugrus beryl. (j–l) Al_2O_3 vs. MgO, FeO, and Na_2O in Abu Rusheid beryl.

The major chemical composition of the studied mica (Table 2) shows a wide range of SiO₂ (38.57–51.15 wt%), Al₂O₃ (10.7–31.24 wt%), FeO (5.85–10.7 wt%), MgO (0.04–20.65 wt%), and K₂O (6.52–11.0 wt%). According to the classification scheme of Foster [36], the analyzed mica spots have compositions between phlogopite and magnesio-biotite, except Abu Rusheid mica, which is mainly plotted in the ferro-muscovite field (Figure 6a). In addition, the studied mica plots are found in the phlogopite field (Figure 6b,c), based on Al^{iv} vs. Fe/Fe+Mg and Al^{vi} vs. Mg/Mg+Fe binary diagrams [37,38]. Using the Mg-Ti-Na triplot diagram that discriminates between primary and secondary mica, the investigated phlogopite occupies the field of secondary mica, while Abu Rusheid muscovite is considered primary mica (Figure 6d).

The analyzed amphibole (Supplementary Table S1a) is a calcic amphibole, with B(Na) < 0.5 and B(Na+Ca) > 1.5. Following the classification scheme of Hawthorne et al. [39], the analyzed amphibole has a composition between magnesiohornblende in orthogneiss and actinolite–tremolite in amphibole schists (Supplementary Figure S1a). It has Mg/(Mg+Fe) and Si cations ranging from 0.94–1.0 to 7.0–8.29, respectively. According to Huang et al. [40], the composition of the investigated magnesiohornblende is consistent with primary amphibole, while tremolite is compatible with secondary amphibole. The analyzed plagioclase ranges in composition from oligoclase in orthogneiss to andesine in biotite schists (Supplementary Table S1a and Figure S1b). According to the classification scheme of Hey [41], the chlorite in phlogopite schists is a Mg-chlorite and is classified as a penninite.

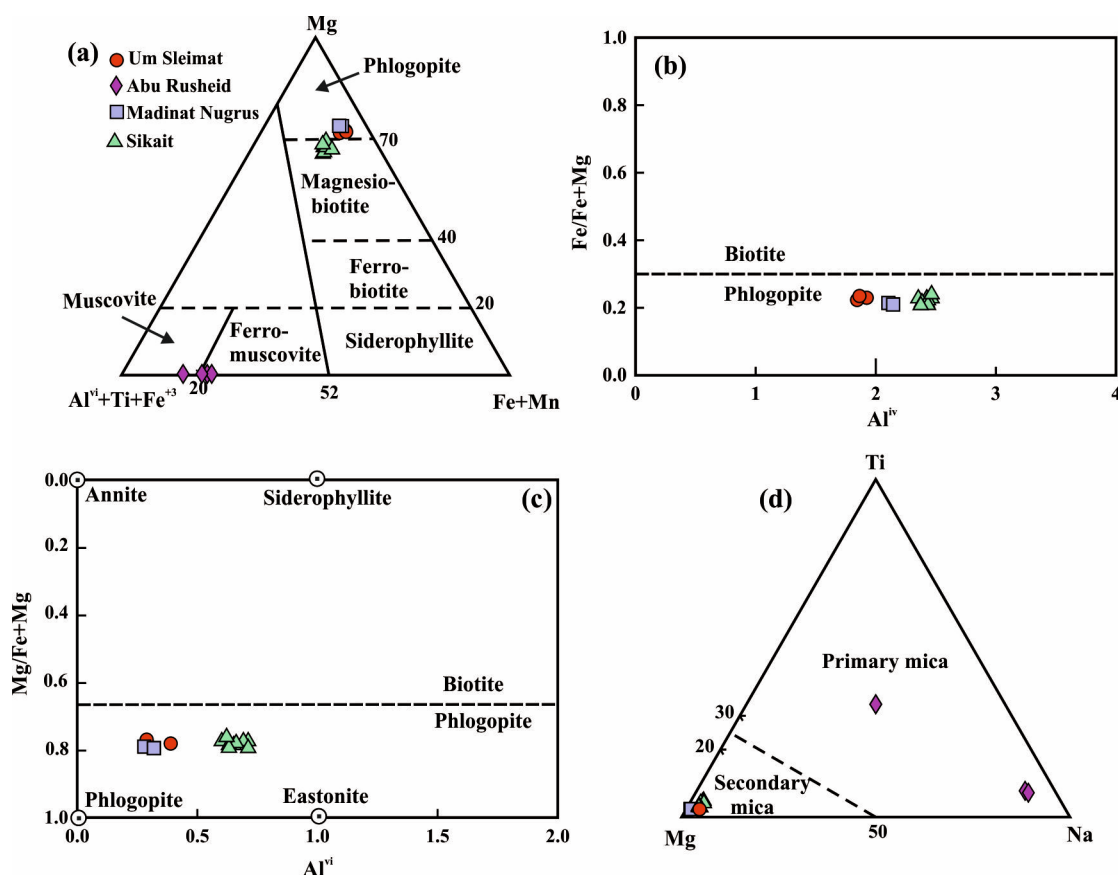


Figure 6. Mica chemistry from pegmatites and mica schists. (a) (Al^{vi} +Ti +Fe⁺³)-Mg-(Fe⁺²+Mn) ternary diagram [36]. (b) Fe/(Fe+Mg) vs. Al^{iv} [37]. (c) Mg/(Fe+Mg) vs. Al^{vi} [37]. (d) Mg-Ti-Na ternary classification diagram [42].

6.1.2. In Situ Trace Element Analysis

In situ analyses of beryl using LA-ICP-MS are given in Table 3 and Supplementary Table S1b. The trace element abundance in the studied beryl is highly variable, even within the same rock sample. Beryl in the Abu Rusheid pegmatite/quartz vein shows notable depletion in Cr (0.2–4.6 ppm) and V (1.7–3.1 ppm), which are rich in beryl from other areas, i.e., Cr: 54–3926 ppm and V: 66–466 ppm. This value of Cr and V is similar to that of emerald from Wadi Nugrus (average Cr: 800 ppm and av. V: 349 ppm) and emeralds from Pakistan (av. Cr: 6635 ppm and av.V: 433 ppm) [2]. In addition, Abu Rusheid beryl is enriched in Zr (31 ppm), Σ REE (7.95 ppm), Th (0.6 ppm), and U (0.3 ppm), compared to those recorded in beryl from other areas (Zr: 0.05–7 ppm; Σ REE: 0.06–2 ppm; Th: 0.0–0.2 ppm; U: 0.01–0.07). The average concentrations of Li (133 ppm), Cs (114 ppm), Rb (73 ppm), and Ni (33 ppm) are higher in Um Sleimat beryl when compared to those of beryl from other areas (Li: 67–79 ppm; Cs: 28–76 ppm; Rb: 7.5–21 ppm; and Ni: 0.7–13.4 ppm). The Cr contents of beryl in Sikait, Madinat Nugrus, and Um Sleimat areas exhibit strong positive correlations with V (Figure 7a–c). In addition, the sum of the V+Cr value is positively correlated with large ion lithophile elements (LILEs: Sr+Rb+Ba+Cs) in Sikait and Madinat Nugrus, while this value exhibits a strong negative correlation with LILEs in Um Sleimat beryl (Figure 7d–f).

The concentration of trace elements changes from core to rim in the zoned beryl crystals (Supplementary Table S1b). In Abu Rusheid beryl, the concentration of Li, Zn, and Rb increases from the core (757 ppm, 536 ppm, and 23 ppm, respectively) to the rim (1014 ppm, 655 ppm, and 32 ppm, respectively). The high concentration of Li (up to 1014 ppm) in Abu Rusheid beryl resembles the highest Li content (average 983 ppm) in emerald from Zimbabwe [43]. On the other hand, in Um Sleimat, the rims of zoned crystals are quite rich in Cr (av. 717 ppm) and Li (av. 134 ppm), but are depleted in V (av. 202 ppm), Cs (av. 115 ppm), and Ti (11 ppm) relative to the cores (av. Cr, 603 ppm; av. Li, 112 ppm; av. V, 246 ppm; av. Cs, 134 ppm; and av. Ti, 19 ppm). In addition, the rims of the zoned beryl crystals in Sikait are enriched in Cr (av. 1989 ppm), V (av. 764 ppm), Li (av.140 ppm), Ni (av. 49 ppm), Zn (av. 27 ppm), Ti (av. 26 ppm), and B (av. 16 ppm), but are poor in Cs (av. 58 ppm) content when compared with the cores (av. Cr, 1208 ppm; av. V, 379 ppm; av. Li, 85 ppm; av. Ni, 10 ppm; av. Zn,13; av. Ti, 13 ppm; av. B, 8; and av. Cs, 108 ppm).

The analyzed beryl shows a wide variation in the concentration of REEs (Σ REEs) among the studied area and even within the same site. For example, the Σ REEs of beryl are 0.04–6.96 ppm in Um Sleimat, 0.04–0.028 ppm in Madinat Nugrus, 0.04–0.07 ppm in Sikait, and 0.03–20 ppm in Abu Rusheid, suggesting a different source of beryl. Chondrite (CI)-normalized REE patterns, using the normalizing values of McDonough and Sun [44], are shown in Figure 8. The investigated beryl crystals exhibit two different REE patterns, classifying them into two types. The first type (type I, Figure 8a) of beryl is enriched in REE (Σ REE), between 3 and 8 times of chondrite, and displays enrichment in LREE relative to flat HREE patterns with $(La/Yb)_N = 8.47$ in Um Sleimat and 8.29 in Abu Rusheid, but its $(Gd/Yb)_N$ ratio is 1.93 of the former and 1.36 of the latter. The type II beryl (Figure 8c,d) is depleted in Σ REE relative to chondrite, and exhibits a concave REE pattern with a positive slope either towards LREEs or HREEs. The abundance of Σ REE increases from type II (0.03–0.23 ppm) to type I beryl (7.0–20 ppm). Likewise, the incompatible elements, including Th and U, pertaining to each type exhibit different distribution patterns (Figure 8b,d).

The in situ trace element analyses of mica (Table 3) indicate that phlogopite in Um Sleimat pegmatite is rich in Rb (165 ppm), Li (113 ppm), Zr (28 ppm), and Σ REE (7.3 ppm) relative to phlogopite in Madinat Nugrus (Rb: 25–41 ppm, Li: 36–66 ppm, Zr: 0.05–1.8 ppm, and Σ REE: 0.4–1 ppm). The trace and REE compositions of the studied phlogopite are comparable to those of metamorphic biotite in metasedimentary rocks (Figure 9a,b). In addition, the spider and REE patterns (Figure 9c,d) of Abu Rusheid muscovite resemble those of magmatic muscovite in leucogranite in Spain [45]

Table 3. Representative in situ analyses (ppm) of beryl, phlogopite, and musovite.

Location	Um Sleimat				Madinat Nugrus				Sikait			Abu Rusheid			
Rock Type	Pegmatite-Related Quartz v.				Phlogopite Schist				Quartz Vein			Pegmatite Vein			
Sample No.	S2				D1				K1			1MK		Mk	1MK
Spot No.	Eu.gr.286	288	287	224	226	225	227	234	235	236	241	244	246	248	
Mineral	Beryl		Phlogopite	Beryl		Phlogopite		Beryl			Beryl		Muscovite		
Li	177.27	84.22	112.86	90.61	76.05	36.26	65.65	73.97	62.33	66.06	65.50	14.69	68.15	30.97	
B	3.67	1.15	3.39	1.91	1.41	1.01	1.87	2.00	1.49	2.35	6.13	12.08	1.19	33.68	
Sc	9.00	281.60	6.60	348.88	286.85	2.43	18.57	171.11	208.33	274.40	10.43	5.98	38.06	12.53	
Nb	3.29	0.05	2.83	0.04	0.11	0.92	1.36	0.04	0.03	0.01	0.65	1.06	0.03	0.22	
Ti	1594.0	333.7	1203.0	441.7	330.2	433.7	713.5	244.4	232.5	266.1	196.9	259.4	200.6	634.2	
Cr	54.07	247.09	45.10	153.80	265.84	12.79	98.59	270.7	481.2	354.7	3.29	4.59	0.20	0.53	
V	65.93	348.80	54.82	269.10	278.97	10.32	17.42	258.4	349.0	293.5	1.79	3.14	0.76	5.19	
Co	20.48	2.07	14.68	2.66	2.08	4.28	7.89	1.22	1.49	1.99	0.17	0.36	0.08	0.20	
Ni	105.19	9.68	76.51	10.60	7.34	25.94	34.05	7.95	19.17	12.99	0.42	0.81	0.13	0.64	
Rb	244.54	18.79	165.00	6.53	9.08	25.36	40.87	3.99	5.03	10.11	19.49	26.31	8.03	40.49	
Sr	11.80	0.19	12.17	0.35	0.31	30.28	3.52	0.02	0.03	0.18	18.72	30.23	0.08	0.32	
Y	1.19	0.03	1.21	0.04	0.10	0.13	0.16	0.05	0.05	0.01	2.10	3.39	0.01	0.34	
Zr	27.21	0.25	27.54	0.47	5.91	1.78	0.05	0.09	0.01	b.d.1	46.75	76.47	0.10	0.14	
Cs	25.96	160.42	18.68	64.06	81.90	3.95	36.69	36.65	80.29	61.63	22.90	1.95	15.30	58.19	
Ba	329.11	3.97	273.46	1.39	8.46	116.27	127.89	0.07	0.14	b.d.1	107.36	180.30	0.31	20.36	
La	1.486	0.023	1.545	0.058	0.026	0.406	0.157	0.002	0.003	0.000	2.523	4.142	0.007	1.381	
Ce	2.659	0.034	2.977	0.009	0.089	0.046	0.015	0.004	0.007	b.d.1	4.611	8.551	0.015	0.256	
Pr	0.329	0.004	0.349	0.017	0.001	0.083	0.031	0.001	0.001	b.d.1	0.565	0.940	0.002	0.449	
Nd	1.356	0.015	1.313	0.075	0.017	0.371	0.117	0.003	0.003	b.d.1	2.204	3.544	0.008	1.320	
Sm	0.264	0.003	0.260	0.011	0.002	0.057	0.023	0.001	0.003	0.004	0.402	0.696	0.001	0.229	
Eu	0.072	0.001	0.068	0.001	0.001	0.012	0.015	0.001	0.000	0.001	0.098	0.184	0.001	0.008	
Gd	0.284	0.003	0.206	0.005	0.002	0.030	0.033	0.005	0.003	0.005	0.347	0.548	0.001	0.124	
Tb	0.027	n.d	0.028	0.000	0.001	0.003	0.003	0.003	0.001	b.d.1	0.050	0.084	b.d.1	0.018	
Dy	0.188	0.008	0.185	0.007	0.008	0.017	0.019	0.004	0.012	0.002	0.315	0.517	b.d.1	0.080	
Ho	0.038	0.000	0.041	0.001	0.002	0.003	0.003	0.001	0.002	b.d.1	0.070	0.110	0.001	0.013	
Er	0.115	0.003	0.110	0.002	0.018	0.012	0.003	0.007	0.006	b.d.1	0.210	0.327	b.d.1	0.040	
Tm	0.020	0.002	0.015	0.002	0.005	0.003	n.d	0.001	0.001	0.001	0.039	0.043	b.d.1	0.006	
Yb	0.119	0.029	0.142	0.050	0.085	0.024	0.007	0.014	0.020	0.022	0.207	0.341	0.001	0.045	
Lu	0.018	0.008	0.020	0.015	0.022	0.006	0.002	0.005	0.008	0.010	0.034	0.049	b.d.1	0.008	
Hf	0.711	0.011	0.791	0.064	0.558	0.152	0.015	0.001	b.d.1	0.009	1.165	1.907	0.034	0.607	
Ta	0.156	0.003	0.118	0.008	0.005	0.041	0.375	0.001	0.003	0.002	0.064	0.111	0.074	0.070	
Pb	5.56	0.07	4.59	0.03	0.11	0.79	1.12	0.02	0.02	0.00	2.63	6.54	0.02	1.46	
Th	0.582	0.005	0.621	0.015	0.012	0.057	0.599	0.001	0.003	b.d.1	0.804	1.468	0.003	0.060	
U	0.216	0.002	0.214	0.004	0.026	0.083	0.160	0.004	0.006	b.d.1	0.308	0.680	0.005	0.092	

Table 3. Cont.

Location	Um Sleimat				Madinat Nugrus			Sikait			Abu Rusheid			
Rock Type	Pegmatite-Related Quartz v.				Phlogopite Schist			Quartz Vein			Pegmatite Vein			
Sample No.	S2				D1			K1			1MK	Mk	1MK	
Spot No.	Eu.gr.286	288	287	224	226	225	227	234	235	236	241	244	246	248
Mineral	Beryl		Phlogopite	Beryl	Phlogopite			Beryl	Beryl			Muscovite		
Σ REE	6.98	0.13	7.26	0.25	0.28	1.07	0.43	0.05	0.07	0.04	11.67	20.08	0.04	3.98
Σ LREE	6.45	0.08	6.72	0.18	0.14	1.01	0.39	0.02	0.02	0.01	10.75	18.60	0.03	3.77
Σ HREE	0.53	0.05	0.54	0.08	0.14	0.07	0.04	0.03	0.05	0.03	0.92	1.47	0.00	0.21
(La/Yb) _N	8.465	0.520	7.394	0.799	0.207	11.732	15.417	0.100	0.090	0.002	8.292	8.257	4.577	20.747
(Gd/Yb) _N	1.928	0.093	1.175	0.079	0.015	1.046	3.857	0.268	0.139	0.185	1.359	1.302	0.405	2.224
Eu/Eu*	0.800	1.172	0.902	0.586	1.571	0.862	1.716	2.790	0.455	0.452	0.803	0.905	1.873	0.151

n.d: not analyzed; b.d.l: below detection limits; Eu.gr: Euhedral grain.

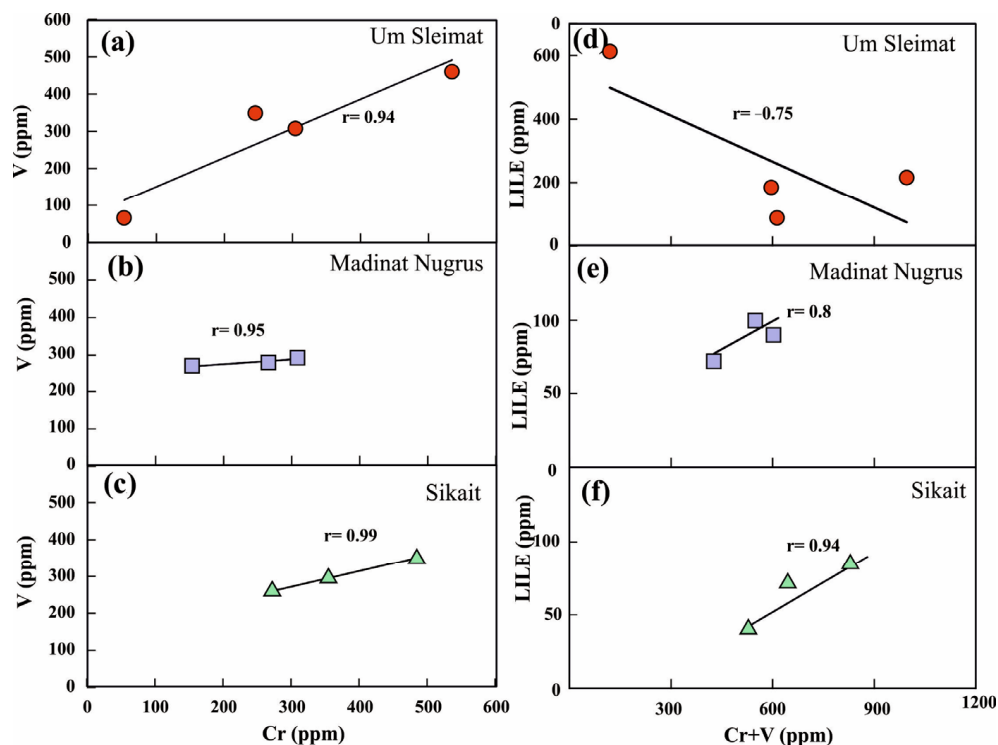


Figure 7. In situ trace elements in emerald from pegmatites. (a–c) Cr vs. V in Um Sleimat, Madinat Nugrus, and Sikait, respectively. (d–f) (Cr+V) vs. LILEs (Ba+Rb+Cs+Sr) in Um Sleimat, Madinat Nugrus, and Sikait, respectively.

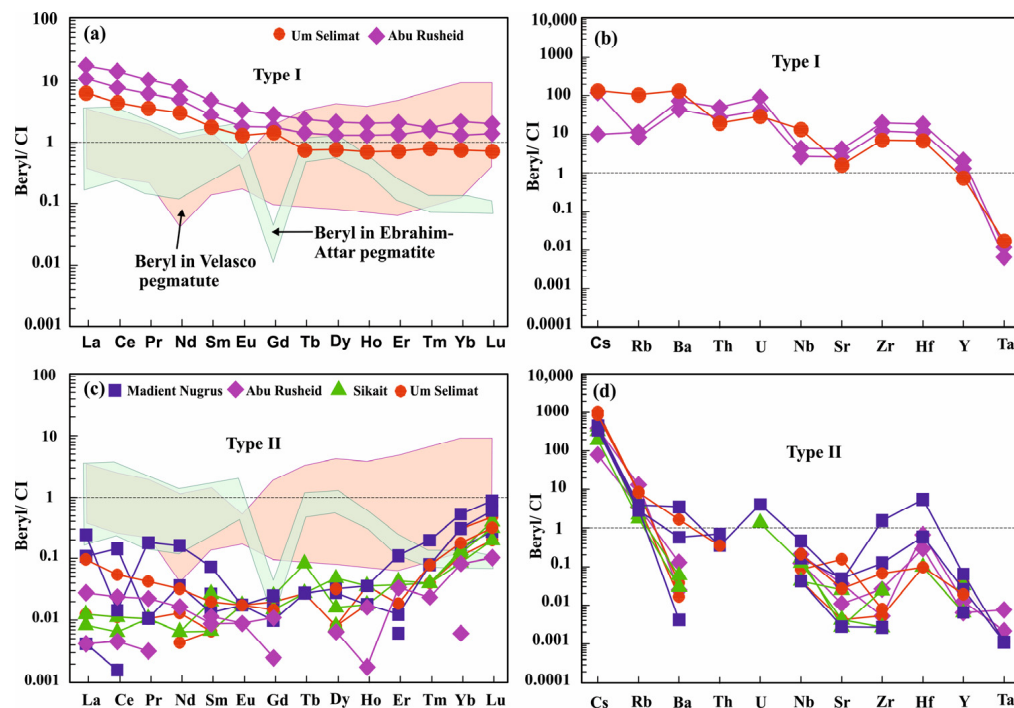


Figure 8. In situ trace and REE elements in emerald/beryl from pegmatites. (a,c) Chondrite (C1)-normalized REE patterns. (b,d) Chondrite (C1)-normalized compatible elements. C1-normalized values follow McDonough and Sun [44]. The field of beryl in Ebrahim-Attar granite is from Azizi et al. [46], the field of beryl in Velasco pegmatite is from Sardi and Heimann [47], and the field of psammittic gneiss is from Hilmy et al. [48].

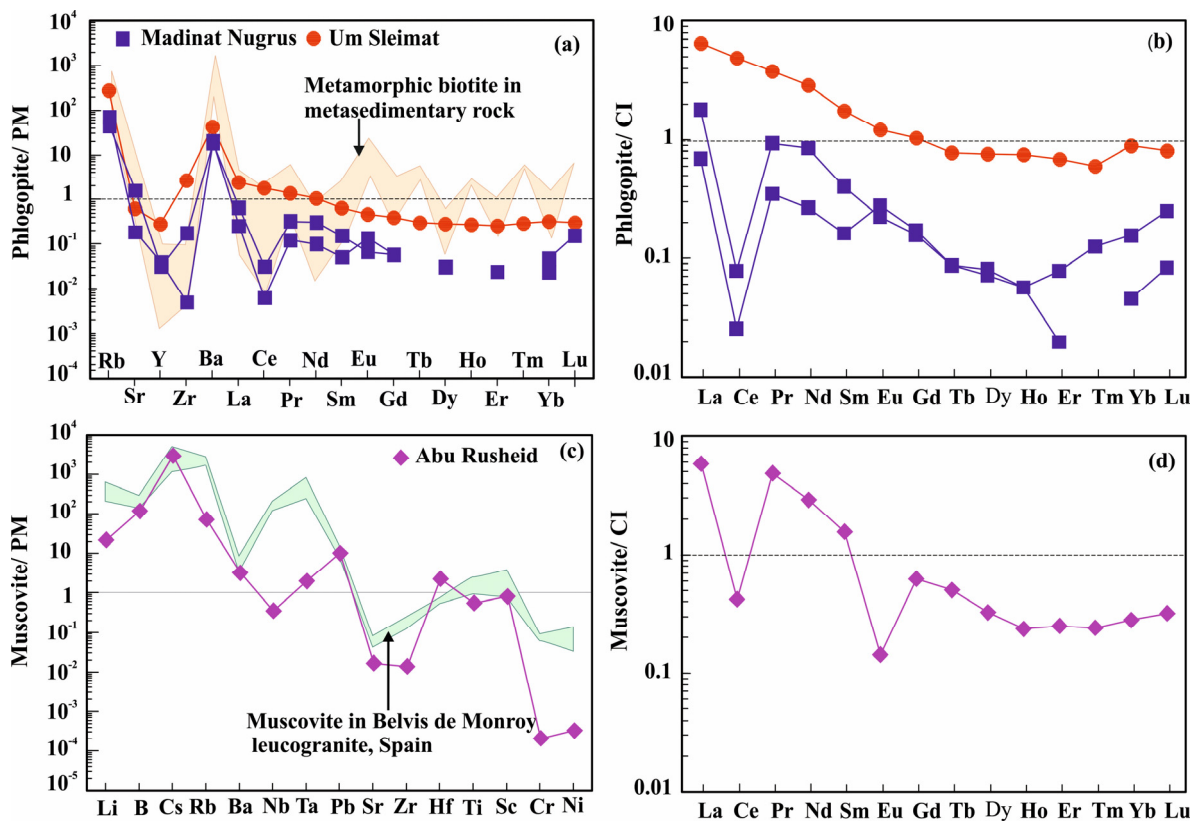


Figure 9. In situ trace and REE elements in phlogopite and muscovite from pegmatites. (a,c) Patterns of primitive mantle (PM)-normalized trace and REE elements. (b,d) Chondrite (C1)-normalized compatible elements. PM- and C1-normalized values follow McDonough and Sun [44]. The field of metamorphic biotite in metasedimentary rocks is from Samadi et al. [49], and the field of muscovite in Belvis de Monroy leucogranite (Spain) is from Merino et al. [45].

7. Discussion

7.1. Pressure-Temperature Condition of Beryl Formation

To obtain a clear insight into the Be mineralization process, it is important to understand the physicochemical conditions under which hydrothermal fluids originate and evolve. The investigated secondary phlogopite can be used to decipher the physicochemical conditions that can be attributed to the hydrothermal systems [50–52], and may consequently provide valuable information regarding the coexisting Be mineralization and alteration conditions [51,53,54]. According to Luhr et al. [55], the calculated temperature of the investigated phlogopite ranges from 592 °C to 702 °C. This temperature range is possibly for the studied beryl, where the temperature for maximum beryl solubility is ~535 °C at 300 MPa and increases to approximately 600 °C at 800 MPa, according to experimental studies on the phase equilibria of the beryl system [56]. In addition, experimental studies conducted on beryl-bearing pegmatites yielded crystallization P-T conditions between 600 and 720 °C at about 2 kbar [57,58]. Also, the crystallization temperature of the Ebrahim-Attar granitic pegmatite-hosted beryl ranges from 586 to 755 °C (average = 629 °C) [8]. This is consistent with the temperature range, 592 °C–702 °C, of the studied beryl and associated phlogopite. The oxidizing/reducing conditions of phlogopite formation can be determined based on its oxygen fugacity (f_{O_2}), which can be estimated using the Fe^{3+}/Fe^{2+} ratio (Table 2; [59]). This oxygen fugacity (f_{O_2}) was calculated based on MagMin_PT (Excel-based mineral sheet) following Gündüz and Asan [60]. The values of estimated f_{O_2} (–21 to –17) and the elevated temperature range suggest that the studied phlogopite is formed under oxidizing and hydrous conditions.

The temperature of tremolite can be estimated using the empirical equation suggested by Gerya et al. [61] as follows: $T\text{ }^{\circ}\text{C} = 389 + [5098.36 * Ti\text{ (p.f.u.)}]$ for $Ti < 0.05$ (p.f.u). The investigated tremolite associated with beryl was formed at temperatures ranging from 415 to 451 °C, suggesting its secondary origin after primary amphibole (e.g., magnesiohornblende). This tremolite was formed after type I beryl, and can possibly be associated with the formation of type II beryl at a temperature range of 400–450 °C. This is consistent with the laboratory work that has estimated beryl temperature's of 400 °C in the presence of H₂O and more hydrous conditions [62].

7.2. Genesis of Beryl and Source of Beryllium

The genesis of beryl is controversial, whereas several deposits are hosted by metamorphic rocks. Most beryl deposits require the coexisting of Cr (\pm V) and Be. Beryllium is a typical incompatible rare element and tends to be concentrated in late-stage crystallization [63], especially in pegmatites and quartz veins (Figures 2 and 3). The BeO, FeO^t, Cr₂O₃, and MgO contents of the studied beryl (Table 1) resemble those of beryl from Egypt [35]. Based on the FeO^t-Cr₂O₃-MgO ternary diagram (Figure 10a), the Abu Rusheid beryl is plotted in the granite-related field, while beryl from Sikait, Madinat Nugrus, and Um Sleimat lies in the schist-related field. All beryl data are plotted in the overlap field of magmatic and hydrothermal beryl (Figure 10b). Therefore, the composition of the investigated beryl deposits (Figure 10a), as well as the geological features of their host rocks, indicate two types of beryl mineralization in the studied area as follows: (1) granite-related beryl (type I; Figure 8a,b) in Abu Rusheid pegmatites and pegmatite-related quartz-bearing beryl, arising from the exsolution of pegmatitic-derived fluids in Um Sleimat (Figure 2), and (2) schist-related emerald in quartz veins from Sikait, Um Sleimat, and Madinat Nugrus (type II; Figure 8c,d). These two types of beryl are similar in morphology and chemical compositions to some beryl samples from across the globe. Fe-Rb, Fe-Cs, Rb-Cs, and Li-Fe discrimination diagrams (Figure 11) can be used to observe if there is a match between the genesis and composition of the studied beryl and those of the beryl from across the world [64]. The analyzed beryl spots from Madinat Nugrus, Um Sleimat, and Sikait fall within the field of Brazil beryl in the four binary diagrams (Figure 11). The formation of beryl deposits in Brazil have been attributed to the interaction of pegmatitic fluids and metamorphic mafic-ultramafic rocks [64,65]. Abu Rusheid beryl data only occupy the Brazil beryl field based on the Rb-Cs (Figure 11c) variation diagram, while, in the other three diagrams, beryl spots are distributed among China, Zambia, Brazil, Afghanistan, and Madagascar beryl (Figure 11a,b,d). In addition, the Na, Cs, and Li contents of beryl can be used to indicate the geochemical features and genesis of its source fluids [66]. On the Li/Cs–Na/Li variation diagram (Figure 12), Abu Rusheid beryl is different in composition from beryl in Sikait and Madinat Nugrus. In Abu Rusheid, Li/Cs shows a significant positive correlation with Na/Li, while beryl from other places is negatively correlated with Na/Li, suggesting compositionally different fluids. Furthermore, the enrichment of the Li/Cs ratio in Abu Rusheid beryl relative to other beryl analyses could be ascribed to the fractional crystallization of the parental melts (e.g., [67]).

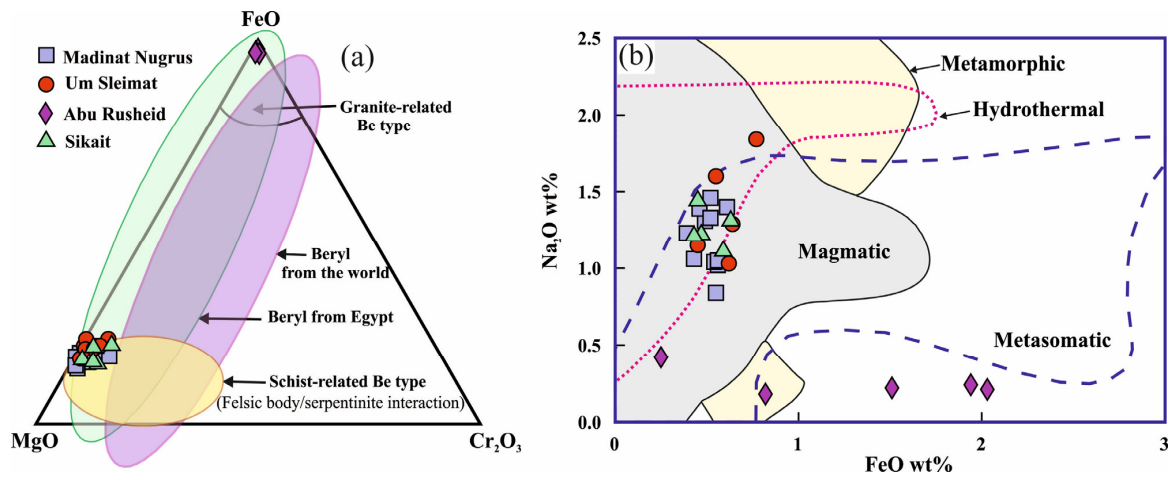


Figure 10. Beryl chemistry from pegmatites. (a) MgO-FeO^t-Cr₂O₃ triplot [35]. The schist-related and granite-related fields are from Mokhtar et al. [68]. (b) Na₂O vs. FeO (wt%), from Merino et al. [45].

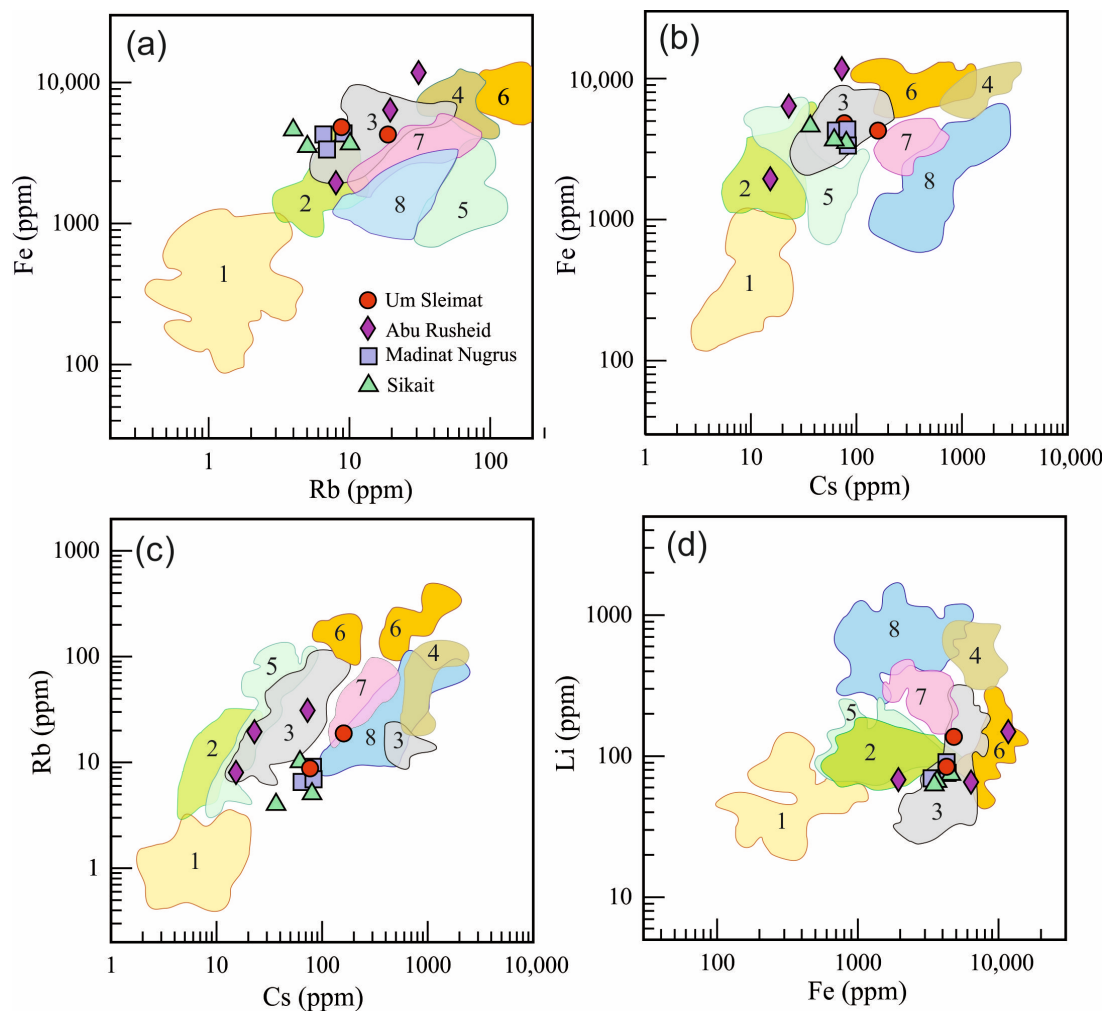


Figure 11. Trace and minor elements (ppm) of beryl. (a) Fe vs. Rb binary diagram. (b) Fe vs. Cs. (c) Rb vs. Cs. (d) Li vs. Fe. The binary discrimination diagrams show the relationships of trace and minor elements (ppm) of the studied beryl in the SED in Egypt and beryl from various localities [64]. Compositional fields of beryl from various occurrences: 1—Colombia; 2—China; 3—Brazil; 4—Zambia; 5—Afghanistan; 6—Madagascar; 7—Ethiopia; 8—Russia (Urals).

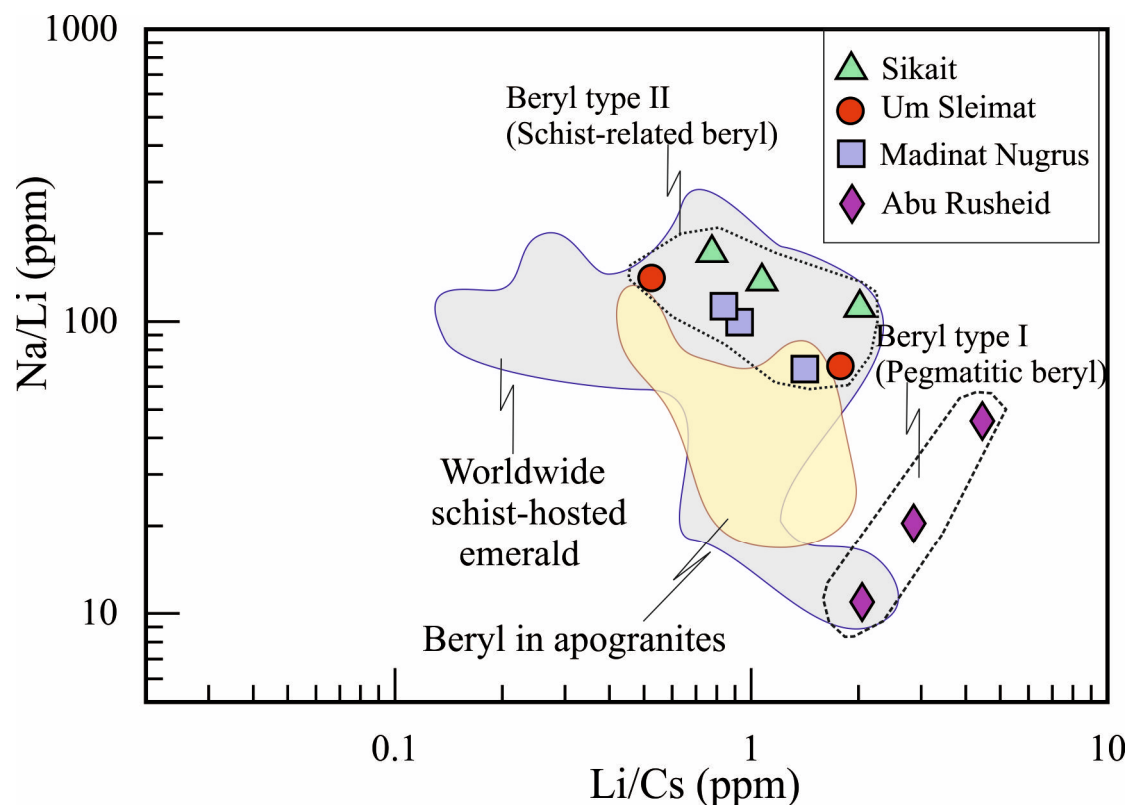


Figure 12. The Li/Cs versus Na/Li variation diagram indicates beryl genesis and its source fluids [46]. Beryl in apogranites in the Eastern Desert of Egypt [63] and schist-hosted emerald [43] are used for comparison. Abu Rusheid euhedral beryl (type I) is different in origin from beryl-related schists (type II) in other places.

The beryl (type I; Figure 8a,b) in Abu Rusheid pegmatites and pegmatitic quartz veins is typically euhedral with six-sided crystals, and forms a triple junction boundary with other silicates (Figure 3a,b), suggesting a magmatic-related origin. It shows notable depletion in MgO (up to 0.01 wt%) and Cr₂O₃ (up to 0.03 ppm), but is rich in REEs that exhibit almost flat patterns (Figure 8a,b) relative to beryl compositions in other places (Figure 1b), reflecting its granitic origin (e.g., [68]). This Abu Rusheid beryl is not only rich in LREE relative to HREE (Figure 8a), but also rich in Ba, Rb, Th, and U (Figure 8b). In contrast, the beryl core is rich in Cs and Ti, being inherited features from its primitive source. This beryl is also enriched in FeO (up to 2.0 wt%) relative to type II beryl, and this is consistent with the considerably high degree of Fe⁺² substitution at the octahedral site in beryl (Figure 5k). The high REE (11.7–20 ppm; Supplementary Table S1b) and FeO contents of Abu Rusheid euhedral six-sided beryl are slightly similar to those of magmatic beryl (Σ REE: ~4.9 ppm; FeO: ~1.18 wt%) in the Ebrahim-Attar granitic pegmatite [8], which crystallized from the primary poor evolved magma produced via the partial melting of the upper continental crust and beryl-bearing (rich in Fe, Na, and H₂O) granitoids in the Eastern Desert of Egypt [63]. Moreover, on the FeO vs. Na₂O binary diagram (Figure 5b), most Abu Rusheid beryl crystals are plotted outside the metasomatic and hydrothermal fields, reflecting their magmatic nature. Only two beryl crystals near the metasomatic field indicate their formation through the mobilization of pre-existing magmatic beryl with late pegmatitic fluids [9,10,69]. The Abu Rusheid euhedral beryl in granitic pegmatite possibly originates from the early phase of the late-stage magmatic-derived fluids (Be-rich fluids) from granite and related pegmatites during the rock–fluid interaction (Figure 8a,b). The REEs, Nb, Ta, Rb, Be, Li, and Cs in these late stage fluids/melts increase gradually during the progress of the crystal fractionation from granite to pegmatite (e.g., [70]). Abu Rusheid pegmatite is directly connected to the apical part of the granitic batholith (Figure 13).

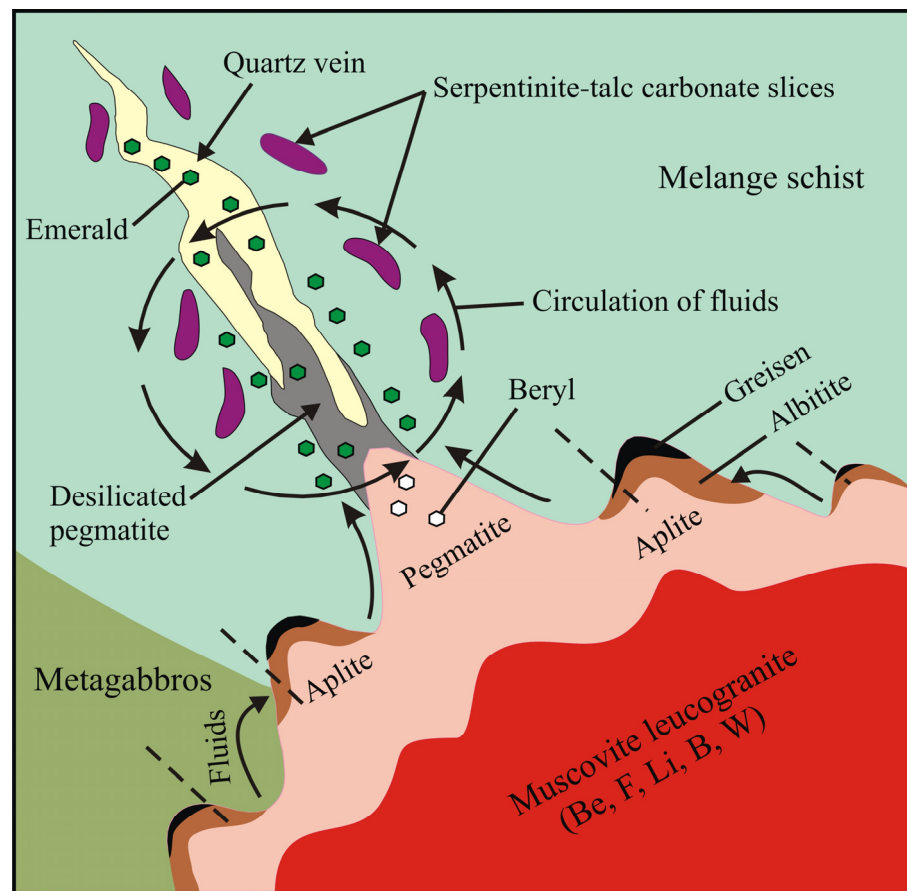


Figure 13. Schematic sketch showing the genetic model for the genesis of beryl in the studied area (modified after Giuliani et al. [3]). The model is based on the emplacement in the leucogranite massif, with its beryl-bearing pegmatite in M-UM rock units represented by mica schists and serpentinites. The fluid circulations from the granite into the surrounding rocks and granitic dykes (arrows), preferentially along the contacts between the pegmatite transform the schistose rocks into a magnesium-rich biotite schist and the pegmatite into a desilicated pegmatite.

On the other hand, two genetic models have been proposed for schist-related emerald mineralization in the SED of Egypt, including the following: (1) metamorphic [71–73] origin and (2) exometamorphic origin [11,19,74]. Grundmann and Morteani [71,72] suggested a pure metamorphic origin for the Egyptian schist-related emerald deposits. Their presumption was based on geochemical and microstructural features, as well as geological investigations, where emerald deposits are restricted to blackwall zones developed at the contact between the tectonically juxtaposed schist and ultramafic rocks during low grade regional metamorphism. However, the absence of significant Be concentration in schists [31] may exclude the formation of beryl during regional metamorphism. Moreover, the very low content of Be in gneiss (1.9–2.2 ppm; [75]) excludes any genetic relation of beryl to being of gneiss origin (metamorphic origin). Furthermore, the geological and geochemical features of the emerald deposits in Egypt argue against such a pure metamorphic origin, emphasizing the role of pegmatitic-derived fluids for beryl mineralization [2,6,7,11,18,63,72,75,76].

The exometamorphic model has also been proposed for schist-related emeralds in the SED of Egypt [11,19], where the crystallization of emerald is a result of the interaction of hydrothermal fluids from parental magmas of felsic rocks and Cr-bearing mafic-ultramafic rocks [31,76]. The mode of the occurrence and chemical composition (Figure 8c,d) of the studied emerald in phlogopite schists (Figure 2c,d) associated with ophiolitic rocks in Sikait, Madinat Nugrus, and Um Sleimat suggest that this emerald origin is possibly related to the interaction of granitic/pegmatitic-derived Be-bearing fluids with pre-

existing mafic-ultramafic rocks (e.g., gabbro, serpentinite, talc carbonate) (Figure 1b) in the ophiolitic mélange. The investigated quartz veins in the mélange schists in Sikait, Madinat Nugrus, and Um Sleimat are spatially related to the proximal garnet muscovite leucogranite (Figure 13). Accordingly, the frequent beryl mineralization in these quartz veins suggests that granite and associated pegmatites are the source rocks for the Be-bearing fluids. This is consistent with the significant concentration of Be in granitic pegmatites (604–1700 ppm; [77]) and peraluminous granite (6 ppm; [7,27]) in the studied area. The granitic rocks and spatially related pegmatites intrude the pre-existing ophiolitic metagabbro and volcanoclastic metasediment (e.g., schist as a matrix of mélange), including slices of serpentinite. The emplacement of these granitic plutons is syn-tectonic with respect to the major ductile Nugrus shear zone, along which the mélange schist and underlying orthogneiss are highly folded. Moreover, Soliman [76] related most of the beryl mineralization to pneumatolytic hydrothermal Be-bearing fluids associated with the episodic emplacement of granites during the Precambrian age along NW-SE trending deep-seated shear zones, such as the Nugrus thrust fault (Figure 1b).

The high MgO content (up to 2.71 wt%; Supplementary Table S1a) of emerald in schists from Sikait, Um Sleimat, and Madinat Nugrus suggests an exometamorphic environment for the genesis of beryl in these areas (e.g., [78]). In addition, on the FeO vs. Na₂O binary diagram (Figure 10b), beryl from Sikait, Um Sleimat, and Madinat Nugrus occupies the overlap between hydrothermal and metasomatic fields that crosscut with the magmatic one, suggesting its source as a magmatic-derived hydrothermal fluid. This is further indicated by the metasomatic substitution of the octahedral Al³⁺ site in beryl by Fe, Mg, and Na (Figure 5). The main source of Mg and Fe is the adjacent serpentinite and schistose rocks, while Na originated from the berylliferous granite crosscutting these rocks. In addition, the significant enrichment of the studied pegmatites in K (K₂O/Na₂O = 2.5–6; [79]), as well as the restriction of post-magmatic alterations, such as albitization (Figure 4d), dominant phlogopite, and muscovite blebs (Figures 3c–f and 4d,e), and the greisenization to the apical parts of leucogranite batholith [11] (Figure 13), all suggest dominant K-metasomatism. This is supported by the high contents of fluid mobile elements (Σ Li+Rb+Cs+Sr: 73–980 ppm; Supplementary Table S1b) of the investigated beryl, reflecting the role of the alkali solution and alkali metasomatism during the emerald formation. The K-rich fluids are possibly related to the leucogranite emplacement (Figure 13) and are responsible for the formation of emerald (Cr-beryl) in quartz veins crosscutting both schist (Figure 2a,b) sequences and intercalated serpentinite bands in Sikait, Madinat Nugrus, and Um Sleimat. The K-rich fluids interact with Be-rich leucogranites, which intruded into schists and carry Be with them. Such Be-bearing fluids infiltrate into the adjacent permeable schists, causing the pervasive metasomatism of serpentinites and schists into talc carbonate and phlogopite schists, with the liberation of Li, Fe, Ca, Mg, Cr, and V into hydrothermal fluids, causing the formation of green emerald (Figure 13). The circulation of these hydrothermal fluids may enhance along the shear zones and thrust faults, like the Nugrus NW-SE trend of the studied area (Figure 1b). Therefore, numerous lenticular beryl-bearing pegmatite pods and quartz veins crosscut the schists along the NW trending shear zone.

The geochemical behavior of the REEs of the investigated beryl, as well as its associated phlogopite, can be used to constrain the evolution of magmatic and hydrothermal systems. The different REE patterns of beryl (Figure 8) and phlogopite (Figure 9a,b) between the different sites in the studied area, and even within the same place, indicate two-stage beryl formation and different compositions of Be-bearing fluids (two heterogeneous fluid cycles). The early phase of the late-stage magmatic-derived fluids was enriched in REEs, U, Th, and LILEs (ex., Cs, Rb, Ba, and Sr, Figure 8a,b; Supplementary Table S1b) when compared with the late phase of these fluids when intermixed with the metamorphic fluids. Type I beryl may have been formed from the early phase of the late-stage magmatic-derived fluids associated with pegmatite formation/emplacement. Some of these fluids (Be-rich fluids) interact with pegmatites, forming in situ beryl, as indicated in Abu Rusheid type I beryl, which may be a magmatic phase associated with pegmatite crystallization (Figure 8a,b).

During the formation of this pegmatite, volatile phases, comprising F, Li, H₂O, and CO₂, play a vital role in the accumulation of Be and the formation of beryl [11]. Fluorine forms stable complexes with Be, potentially leading to the accumulation of beryl in the late crystallization stage [80,81]. The volatile F is produced from the decomposition of biotite or amphibole during the partial melting of the lower crust [82,83], and this explains why our beryl mineralization is mainly associated with mica in F-rich phases (Figures 3 and 4). For the formation of Abu Rusheid beryl II, the late phase of the late-stage magmatic-derived fluids of pegmatite emplacement was diluted in compositions with other metamorphic fluids, and becomes more depleted in REEs, U, Th, and LILEs. These resultant hydrothermal fluids react again with Abu Rusheid pegmatites, forming type II beryl (Figure 8c,d) in some Abu Rusheid samples. This is consistent with the petrographic investigation of desilicated pegmatite in Abu Rusheid. In the other places, such as Wadi Sikait, Madinat Nugrus, and Um Sleimat (Figure 1b), the late phase of the late-stage magmatic-derived fluids (highly Be-rich) was intermixed with the serpentinite/schist-derived fluids during the rock–fluid interaction, forming Cr-rich beryl or emeralds (type II; Figure 8c,d) and the associated K-rich phlogopites in the studied mica schists.

7.3. Factors Controlling Beryl Distribution in the SED

Beryl mineralization is relatively rare, and may be classified into beryl related to granitic intrusions, or beryl related to schists without pegmatites (e.g., [78,84]). Following this classification scheme, two modes of beryl occurrences are recognized in the SED of Egypt as follows: (1) schist-related emerald and (2) granite-related beryl of the Neoproterozoic age [2,6,7,11,18,63,68,72,75,85,86].

Beryl mineralization in the SED of Egypt is restricted to the intrusive contact between orthogneiss and/or biotite granite and the overlying phlogopite schist. The most studied beryl deposits are closely related to pegmatite veins crosscutting schists (Figure 2), and are controlled by tectonic structures, such as thrust faults and shear zones, like the studied beryl along the Nugrus shear zone (Figure 1b). For instance, the beryl-bearing schist zone (dominant in this study) extends for some 45 km in the NW trend along the Nugrus thrust [87] (Figure 1b). The beryl is commonly restricted in the mica schist as a *mélange* matrix, in which subordinate slices of amphibolite and serpentinite are imbricated. Beryl also occurs in quartz and pegmatite veins (Figure 2), where numerous lenticular pegmatite pods and quartz veins crosscut schists along the NW trending shear zone. In some places, garnet-muscovite-leucogranitic plutons and spatially related aureoles of pegmatitic veins intruded this sequence along the Nugrus shear zone with NNW to NW-SE trends [87] (Figure 1b).

Granite-related beryl is also recorded in Abu Rusheid; this beryl mineralization is associated with post-orogenic granitoids that are enriched in Li, Rb, Cs, Be, Nb, Ta, REEs, Sn, U, Th, Zr, and Y. These granitoids were formed either through autometamorphic, post-magmatic alteration processes (e.g., apogranite, [88]), or by fractional crystallization from melts enriched in F and Li (e.g., Li-albite granites; [89]). The granite-related disseminated beryl occurs in pegmatoidal lenses and veins, greisens, and quartz veins (Figure 2).

The distribution of beryl deposits is controlled by several factors, including the following: (1) the type of geologic environment, whether magmatic or metamorphic; (2) the type of host rocks; (3) the degree of metamorphism; (4) the style of mineralization; and (5) the type, composition, temperature, and pressure of the fluids [3,72]. These factors can explain why the distribution of beryl deposits in the SED of Egypt is not haphazard. The beryl mineralization in the SED is restricted to definite rock types (schistose matrix of ophiolitic *mélange* and pegmatites; Figures 1 and 2) and associated mineral assemblages (quartz, phlogopite, biotite, muscovite, amphibole, chlorite, fluorite, tourmaline...etc.; Figure 3). These host rocks and mineral assemblages of beryl are in agreement with the most frequent source rocks of Be, which are high silica crustal granite and their related rocks, such as pegmatites and aplites (e.g., [3,9,10]). Most of the mineral assemblages associated with beryl are secondary minerals, such as phlogopite with high Mg/Fe (>1.5) [38] and actinolite

and chlorite, which originate from alkali hydrothermal metasomatism. The Mg/Fe ratio (3.23–5.96) of the investigated phlogopite argues against its magmatic nature (Mg/Fe < 1) and suggests a hydrothermal origin (Mg/Fe > 1.5) [38]. Consequently, the investigated beryl is enriched in fluid mobile elements (FMEs: Sum of Li, Rb, Cs, Sr: 73–980 ppm; Supplementary Table S1b), especially alkaline elements. The FMEs and hydrous conditions play a critical role in increasing the solubility of Be, which has high solubility in melts/fluids that are rich in H₂O, Cs, Rb, Li, F, and B [58]. This is evidence of the role of hydrothermal fluids and K-metasomatism for beryl formation (e.g., [6,11]). The beryl in the phlogopite schist (Figure 2c,d) occurs close to the contact (about 10 cm) between ultramafic rocks and the intruded pegmatite veins [11,29]. At this contact, significant minerals can be yielded according to metasomatism varieties [6]. Actinolite and phlogopite can be produced via Mg–Ca-metasomatism and K-metasomatism, respectively. The high beryl accumulation along the contact zones of pegmatite with the metasediment matrix (Schist) reflects that beryl is formed from two different fluid circulations, i.e., Be-rich magmatic-derived fluids from muscovite granite/pegmatitic melts, and hydrothermal fluids enriched in Mg, Cr, and V from mafic-ultramafics and schists [2]. These hydrothermal fluids may form emerald within some quartz veins. In addition, the composition of the parent magmas of felsic rocks with highly magmatic-derived fluids (rich in F, Li, W, B, U, Th, Cl, Cs, Rb, Be, and H₂O) and a high degree of magma fractionation (more evolved magma), or late stage melts (forming pegmatite veins) are other factors which possibly influence beryl mineralization. The dominant alkali metasomatism is also essential for the emerald formation (see the previous discussion section). Pegmatites (Figure 2) were formed in the late stage from the more evolved hydrous magmas/melts with enriched Be. The restriction of beryl in quartz veins and pegmatites (Figure 2) supports this conclusion. This is in agreement with the formation of beryl that requires high Be contents during magmatic differentiation and/or hydrothermal processes because of the low Be content (1.9–3.1 ppm) in the crust [90].

The beryl deposits in the Eastern Desert of Egypt are located along faults, thrusts, and shear zones, where Cr- and V-bearing ultramafic rocks are emplaced [91]. This occurrence consists in the investigated beryl mineralization confined to the Nugrus thrust (Figure 1b), which is a ductile shear zone. This major shear zone separates the medium-grade gneiss in the footwall from the low-grade ophiolitic mélangé in the hanging wall [92]. For instance, beryl mineralization in the SED is generally attributed to a NW–SE trending deep-seated tectonic zone of the Precambrian age, and is concentrated in two small belts as follows: (1) the Homret Akarem-Homret Mikpid (HA-HM) district and (2) the Zabara- Um Kabu (Z-UK; Figure 1b) district [7,15,16]. This large area is affected by the Najd strike-slip shear-zone (NW–SE) and its related structure, such as the Nugrus thrust/or shear zone, trending in a NW–SE direction. This Najd shear zone (or the Nugrus shear zone) is not only controlling the distribution of beryl mineralization in the SED of Egypt, but also structurally controls the occurrence and accumulation of garnet mineralization, rare metal-bearing granite, and gold concentrations of the Sukari gold mine; this is because this zone is considered a channels for hydrothermal fluids and alterations [93–97]. The Nugrus faults and shear zone (Figure 1b), with the NNW to NW-directed wrench corridor [87], may serve as conduits for the migration and circulation of hydrothermal fluid, which intensifies the hydrothermal alteration of granites and promotes mineral accumulation in a specific zone. This major shear zone enhances the emplacement of mineralized granite plutons and controls an extensive alkali metasomatism, followed by postmagmatic fluids [72,98]. Finally, the occurrence of beryl within major suture or shear zones does not necessarily rule out any connection with the granitic intrusion and its magma-derived fluids (e.g., [99,100]).

8. Conclusions

1. Beryl mineralization collected from Um Sleimat, Madinat Nugrus, Wadi Abu Rusheid, and Wadi Sikait is mainly restricted along the NW–SE Nugrus-Sikait shear zones in the SED of Egypt, providing evidence of structurally controlling the occurrence and distribution of beryl.

2. The beryl mainly occurs as individual crystals and/or aggregates in pegmatites and quartz, as well as pegmatite veins crosscutting the mélange schist and ophiolitic rocks. There are two types of beryl mineralization in the studied area as follows: (1) granite-related beryl (type I) in Abu Rusheid granitic pegmatites and pegmatitic quartz veins, and (2) schist-related emerald (type II) in quartz veins in Sikait, Um Sleimat, and Madinat Nugrus. The granite-related beryl (pegmatitic type) in Wadi Abu Rusheid ranges in color from colorless to pale green, and is mainly restricted in pegmatite veins; it is poor in Cr_2O_3 and MgO (<0.03 wt%). The schist-related beryl from other places is deep green in color and rich in Cr_2O_3 (up to 0.27 wt%) and MgO (up to 2.71 wt%); it is found in quartz veins, phlogopite schists, and amphibole schists.
3. The investigated mica associated with beryl are mainly phlogopites of hydrothermal origin (K metasomatism) and biotites and ferro-muscovites of magmatic nature. Beryl is also enriched in alkali fluid mobile elements (ΣLi , Rb, Cs, and Sr: 73–980 ppm), providing evidence of the role of hydrothermal fluids and K metasomatism in beryl formation and distribution.
4. The change of REE patterns and REE concentrations, including 0.04–6.96 ppm in Um Sleimat, 0.04–0.028 ppm in Madinat Nugrus, 0.04–0.07 ppm in Sikait, and 0.03–20.0 ppm in Abu Rusheid, and the abundance of U, Th, and REEs, which increases from type II to type I beryl, reflect the different sources of beryl and the different compositions of Be-rich fluids which interact with rocks to form beryl deposits.
5. The change in some trace elements in beryl from the core to the rim, where the rims are mainly rich in Li, Rb, and B (fluid mobile elements), not including Cr and Zn, reflects the addition of these mobile elements from hydrothermal fluids to beryl during the formation. In contrast, the beryl core is rich in Cs and Ti, which are inherited features from the primitive fluid/melt sources.
6. Beryl mineralization is related to the interaction between granitic/pegmatitic-derived Be-bearing fluids, which are associated with the episodic emplacement of granite along the NW-SE deep-seated shear zone, and the preexisting ophiolite rocks interlayered with the mélange schist. The euhedral type I beryl crystal in Abu Rusheid may have been formed in situ from the early phase of the late-stage magmatic-derived fluids associated with the pegmatite formation/emplacement, representing a magmatic phase associated with pegmatite crystallization. In the late stage of pegmatite emplacement, the composition of these fluids dilutes with other metamorphic fluids, and then becomes more depleted in REEs, U, Th, and LILEs. These diluted hydrothermal fluids react again with pegmatites, forming type II beryl in Abu Rusheid. In other places, such as Wadi Sikait, Madinat Nugrus, and Um Sleimat, the late phase of the late-stage Be-rich fluids related to granitic pegmatites or granite was mixed with serpentinite/schist-derived fluids during felsic rock intrusions in the ophiolitic mélange, forming emerald in the mica schist. The two beryl types (I and II) reflect two heterogeneous fluid cycles and compositions.
7. The composition of the parent magmas of felsic rocks with highly magmatic-derived fluids (rich in F, Li, W, B, U, Th, Cl, Cs, Rb, Be, and H_2O) and a high degree of magma fractionation (more evolved magma) or the late stage melts (forming pegmatite veins) and fluid compositions (rich in Be, Li, Cs, Rb, K), as well as alkali metasomatism, are other factors possibly holding influence on beryl mineralization. In addition, beryl mineralization is concentrated along linear NW–SE faults, thrusts, and shear zones, such as the Nugrus shear zone, which controls the distribution of beryl mineralization in the SED of Egypt. The Nugrus shear zone may serve as a conduit for the migration and circulation of hydrothermal fluids, which enhance the hydrothermal alteration of granites and promote beryl accumulation in a specific zone.

Supplementary Materials: The following supporting information can be downloaded at: <https://www.mdpi.com/article/10.3390/min14050465/s1>. Supplementary Table S1a: EMPA of beryl, mica (phlogopite, biotite and muscovite), plagioclase, amphibole, quartz, chlorite, rutile, pyroxene and sphene, the SED of Egypt. Supplementary Table S1b: In situ analyses (ppm) of beryl, phlogopite and muscovite in pegmatite veins. Supplementary Figure S1. (a) Amphibole classification diagram [39], (b) Or-Ab-An classification diagram for plagioclase in the schistose mélange rocks [33].

Author Contributions: Conceptualization, M.Z.K. and S.A.E.-S.; methodology, M.Z.K., K.M.A., A.T. and E.T.; validation, M.Z.K., G.M.S., K.A. and S.A.E.-S.; formal analysis, M.Z.K., E.T., A.T., K.M.A. and K.A.; investigation, M.Z.K., G.M.S. and S.A.E.-S.; resources, M.Z.K. and G.M.S.; data curation, M.Z.K. and S.A.E.-S.; writing—original draft preparation, M.Z.K., S.A.E.-S., G.M.S. and K.M.A.; writing—review and editing, M.Z.K. and S.A.E.-S.; visualization, M.Z.K., E.T., A.T. and S.A.E.-S.; supervision, M.Z.K.; project administration, M.Z.K. and K.A.; funding acquisition, K.A. All authors have read and agreed to the published version of the manuscript.

Funding: This research funded by Researchers Supporting Project Number (RSP2024R351), King Saud University, Riyadh, Saudi Arabia.

Data Availability Statement: All data derived from this research are presented in the enclosed figures and tables, as well as Supplementary Table S1 and Supplementary Figure S1.

Acknowledgments: The first author is grateful to all colleagues in the Geology Department at Niigata University (Japan) for their support during his 2019–2020 stay, helping in terms of polishing thin sections, petrography, EDS-SEM, and the mineral chemistry (EPMA) of minerals and ores. The first author is grateful to colleagues at Kanazawa University, Japan, for their support during the in situ analyses of minerals using LA-ICP-MS. All authors thank Moustafa Gharib, passed away, Helwan University, for his support. Deep thanks and gratitude to the Researchers Supporting Project Number (RSP2024R351), King Saud University, Riyadh, Saudi Arabia, for funding this research article.

Conflicts of Interest: The authors declare no conflicts of interest.

References

- Grew, E.S. Mineralogy, petrology and geochemistry of beryllium: An introduction and list of beryllium minerals. *Rev. Mineral. Geochem.* **2002**, *50*, 1–76. [[CrossRef](#)]
- Abdel Gawad, A.E.; Ene, A.; Skublov, S.G.; Gavrilchik, A.K.; Ali, M.A.; Ghoneim, M.M.; Nastavkin, A.V. Trace element geochemistry and genesis of beryl from Wadi Nugrus, South Eastern Desert, Egypt. *Minerals* **2002**, *12*, 206. [[CrossRef](#)]
- Giuliani, G.; Groat, L.A.; Marshall, D.; Fallick, A.E.; Branquet, Y. Emerald deposits: A review and enhanced classification. *Minerals* **2019**, *9*, 105. [[CrossRef](#)]
- Guzmán, J.O. Emerald mining in Sikait: Organization and distribution of emerald production in Roman Egypt. *Pol. Archaeol. Mediterr.* **2020**, *29*, 173–199.
- Karampelas, S.; Gaillou, E.; Herreweghe, A.; Maouche, F.; Hennebois, U.; Leblan, S.; Delaunay, A. Gemological study of an emerald reportedly from Egypt in Paris School of Mines museum. In Proceedings of the 23rd International Mineralogical Association Conference, Lyon, France, 18–22 July 2022.
- Khaleal, F.M.; Lentz, D.R.; Hall, D.C. Mineral chemistry and genesis of emerald and beryl mineralization Desert of Egypt. *Egypt. J. Chem.* **2022**, *65*, 601–623.
- Khaleal, F.M.; Saleh, G.M.; Lasheen, E.S.R.; Lentz, D.R. Occurrences and genesis of emerald and others beryl mineralization in Egypt: A review. *Phys. Chem. Earth Parts A/B/C* **2022**, *128*, 103266. [[CrossRef](#)]
- Daneshvar, N.; Azizi, H.; Asahara, Y.; Tsuboi, M.; Minami, M.; Mohammad, Y.O. Geochemistry and genesis of beryl crystals in the LCT pegmatite type, Ebrahim-Attar mountain, Western Iran. *Minerals* **2021**, *11*, 717. [[CrossRef](#)]
- Giuliani, G.; Cheillett, A.; Zimmermann, J.L.; Ribeiro-Althoff, A.; France-Lanord, C.; Feraud, G. Les gisements d'émeraude du Brésil: Genèse et typologie. *Chron. Rech. Minière* **1997**, *526*, 17–61.
- Giuliani, G.; France-Lanord, C.; Zimmermann, J.L.; Cheillett, A.C.; Coget, P.; Arboleda, C.; Charoy, B.; Coget, P.; Fontan, F.; Giard, D. Composition of fluids, $\delta^{18}O$ of lattice oxygen in beryls: Genetic implications for Brazilian, Colombian and Afghanistani emerald deposits. *Int. Geol. Rev.* **1997**, *39*, 400–424. [[CrossRef](#)]
- Abdalla, H.M.; Mohamed, F.H. Mineralogical and geochemical investigation of emerald and beryl mineralisation, Pan-African Belt of Egypt: Genetic and exploration aspects. *J. Afr. Earth Sci.* **1999**, *28*, 581–598. [[CrossRef](#)]
- Abdalla, H.M.; El-Sayed, A.A.; El-Afandy, A.H. Geochemical and mineralogical investigation of Wadi Ghazala beryl occurrence, SE Sinai, Egypt: An example of abyssal Be-pegmatites. *Egypt J. Geol.* **2001**, *45*, 151–168.
- Beal, K.L.; Lentz, D.R. Aquamarine beryl from Zealand Station, Canada: A mineralogical and stable isotope study. *J. Geosci.* **2010**, *55*, 57–67. [[CrossRef](#)]
- Schwarz, D.; Giuliani, G.; Grundmann, G.; Glas, M. The origin of emerald. *Emeralds World Extralapis Engl.* **2002**, *2*, 18–23.

15. El Shatoury, H.M. Preliminary report on prospecting for mineral deposits of acidic type at Homret Mikpid, Eastern Desert. *Egypt. Intern. Rep. United Nations Dev. Programs UAR Assess. Miner. Potential Aswan Reg.* **1970**, *15*, 1–14.
16. Hassan, M.A.; El Shatoury, H.M. Beryl occurrences in Egypt. *Min. Geol.* **1976**, *26*, 253–262.
17. Kröner, A.; Krüger, J.; Rashwan, A.E.A.A. Age and tectonic setting of granitoid gneisses in the Eastern Desert of Egypt and south-west Sinai. *Geol. Rundsch.* **1994**, *83*, 502–513. [[CrossRef](#)]
18. Omar, S.A.M. Characterization and Evaluation of Some Beryl Occurrences in the Eastern Desert, Egypt. Ph.D. Thesis, Cairo University, Cairo, Egypt, 2001.
19. Sharaky, A.M. Emerald mineralization in Africa: A case study from Marsa Alam district, Egypt. In *Second International Conference of Natural Resources in Africa*; Institute of African Research and Studies, Cairo University: Cairo, Egypt, 2009; p. 21.
20. Harrell, J.A. Archaeological geology of Wadi Sikait, PalArch's. *J. Archaeol. Egypt/Egyptol.* **2006**, *4*, 1–12.
21. Khaleal, F.M. Geologic Evaluation of Some Rare Metal Resources in Nugrus-Sikait Area, Eastern Desert, Egypt. Unpublished. Ph.D. Thesis, Al-Azhar University, Cairo, Egypt, 2005.
22. Ibrahim, I.; Saleh, G.M.; Amer, T.; Mahmoud, F.; Abu El Hassan, A.; Ali, M.A.; Mahmoud, M. Uranium and associated rare metals potentialities of Abu Rusheid brecciated shear zone II, south Eastern Desert, Egypt. *Nucl. Mater. Auth. Cairo Int. Rep.* **2004**, *182*, 1–145.
23. Saleh, G.M. The Potentiality of Uranium Occurrences in Wadi Nugrus Area, South Eastern Desert, Egypt. Ph.D. Thesis, Mansoura University, El Mansoura, Egypt, 1997.
24. Stern, R.J.; Hedge, C.E. Geochronologic and isotopic constraints on late Precambrian crustal evolution in the Eastern Desert of Egypt. *Am. J. Sci.* **1985**, *285*, 97–127. [[CrossRef](#)]
25. Robinson, F.A.; Bonin, B.; Pease, V.; Anderson, J.L. A discussion on the tectonic implications of Ediacaran late- to post- orogenic A-type granite in the northeastern Arabian Shield, Saudi Arabia. *Tectonics* **2017**, *36*, 582–600. [[CrossRef](#)]
26. Saleh, G.M.; Kamar, M.S.; El Saeed, R.L.; Ibrahim, I.H.; Azer, M.K. Whole rock and mineral chemistry of the rare metals-bearing mylonitic rocks, Abu Rusheid borehole, south Eastern Desert, Egypt. *J. Afr. Earth Sci.* **2022**, *196*, 104736. [[CrossRef](#)]
27. Stern, R.J.; Ali, K. Crustal evolution of the Egyptian Precambrian rocks. In *The Geology of Egypt, Regional Geology Reviews*; Hamimi, Z., El-Barkooky, A., Martínez Frías, J., Fritz, H., Abd El-Rahman, Y., Eds.; Springer: Cham, Germany, 2020; pp. 131–151.
28. Khaleal, F.M. Emeralds and other beryls in Egypt: A review. In Proceedings of the Luxor Meeting Organized by the United Nations Economic Commission for Europe (UNECE) in Collaboration with the Nuclear Materials Authority of Egypt (NMA), Luxor, Egypt, 18–22 October 2015; pp. 1–27.
29. Harrell, J.A. Archaeological geology of the world's first emerald mine. *Geosci. Can.* **2004**, *31*, 69–76.
30. Surour, A.A. Petrology, Geochemistry and Mineralization of Some Ultramafic Rocks, Egypt. Ph.D. Thesis, Cairo University, Cairo, Egypt, 1993.
31. El Dougdoug, A.; Takla, M.A.; Surour, A.A.; Hussein, A.A.; El Eraky, F. Mineralogy and origin of Wadi Sikait emerald, south Eastern Desert, Egypt. In Proceedings of the 3rd International Conference on Geochemistry, Kuala Lumpur, Malaysia, 7–11 April 1997; Volume 1, pp. 221–239.
32. Pearce, N.J.G.; Perkins, W.T.; Westgate, J.A.; Gorton, M.P.; Jackson, S.E.; Neal, C.R.; Chenery, S.P. A compilation of new and published major and trace element data for NIST SRM 610 and NIST SRM 612 glass reference materials. *Geostand. Newsl.* **1997**, *21*, 115–144. [[CrossRef](#)]
33. Deer, W.A.; Howie, R.A.; Zussman, J. *The Rock Forming Minerals. Vol. IB*, 2nd ed.; Longman Group Ltd.: London, UK, 1992.
34. Gavrilenko, E.V.; Pérez, B.C.; Bolibar, R.C.; del Amo, D.G. Emeralds from the Delbegetey deposit (Kazakhstan): Mineralogical characteristics and fluid-inclusion study. *Mineral. Mag.* **2006**, *70*, 159–173. [[CrossRef](#)]
35. Hammarstrom, J.M. Mineral chemistry of emeralds and some minerals from Pakistan Afghanistan: An electron microprobe study. In *Emeralds of Pakistan*; Kazmi, A.H., Snee, L.W., Eds.; Van Nostrand Reinhold: New York, NY, USA, 1989; pp. 125–150.
36. Foster, M.D. Interpretation of the composition of trioctahedral micas. *US Geol. Surv. Prof. Pap.* **1960**, *354-B*, 1–146.
37. Deer, W.A.; Howie, R.A.; Zussman, J. *An Introduction to the Rock Forming Minerals*; Longman: London, UK, 1966.
38. Beane, R.E. Biotite stability in the porphyry copper environment. *Econ. Geol.* **1974**, *69*, 241–256. [[CrossRef](#)]
39. Hawthorne, F.C.; Oberti, R.; Harlow, G.E.; Maresch, W.V.; Martin, R.F.; Schumacher, J.C.; Welch, M.D. Nomenclature of the amphibole supergroup. *Am. Miner.* **2012**, *97*, 2031–2048. [[CrossRef](#)]
40. Huang, H.; Fryer, B.J.; Polat, A.; Pan, Y. Amphibole, plagioclase and clinopyroxene geochemistry of the Archean Fiskensæset Complex at Majorqap qáva, southwestern Greenland: Implications for Archean petrogenetic and geodynamic processes. *Precambrian Res.* **2014**, *247*, 64–91. [[CrossRef](#)]
41. Hey, M.H. A new review of the chlorite. *Mineral. Mag. J. Mineral. Soc.* **1954**, *30*, 227. [[CrossRef](#)]
42. Miller, C.F.; Stoddard, E.F.; Bradfish, L.J.; Dollase, W.A. Composition of plutonic muscovite; genetic implications. *Can. Mineral.* **1981**, *19*, 25–34.
43. Aurisicchio, C.; Conte, A.M.; Medeghini, L.; Ottolini, L.; De Vito, C. Major and trace element geochemistry of emerald from several deposits: Implications for genetic models and classification schemes. *Ore Geol. Rev.* **2018**, *94*, 351–366. [[CrossRef](#)]
44. McDonough, W.F.; Sun, S.S. The composition of the Earth. *Chem. Geol.* **1995**, *120*, 223–253. [[CrossRef](#)]
45. Merino, E.; Villaseca, C.; Orejana, D.; Jeffries, T. Gahnite, chrysoberyl and beryl co-occurrence as accessory minerals in a highly evolved peraluminous pluton: The Belvís de Monroy leucogranite (Cáceres, Spain). *Lithos* **2013**, *179*, 137–156. [[CrossRef](#)]

46. Azizi, H.; Mohammadi, K.; Asahara, Y.; Tsuboi, M.; Daneshvar, N.; Mehrabi, B. Strongly peraluminous leucogranite (Ebrahim-Attar granite) as evidence for extensional tectonic regime in the Cretaceous, Sanandaj Sirjan zone, northwest Iran. *Geochemistry* **2016**, *76*, 529–541. [[CrossRef](#)]
47. Sardi, F.G.; Heimann, A. Pegmatitic beryl as indicator of melt evolution: Example from the Velasco district, Pampeana pegmatite province, Argentina, and review of worldwide occurrences. *Can. Mineral.* **2014**, *52*, 809–836. [[CrossRef](#)]
48. Hilmy, M.E.; El-Bayoumi, R.M.; Eid, A.S. Geology, geochemistry and mineralization of the psammitic gneiss of Wadi Abu-Rusheid, Eastern Desert, Egypt. *J. Afr. Earth Sci.* **1990**, *11*, 197–205. [[CrossRef](#)]
49. Samadi, R.; Torabi, G.; Kawabata, H.; Miller, N.R. Biotite as a petrogenetic discriminator: Chemical insights from igneous, meta-igneous and meta-sedimentary rocks in Iran. *Lithos* **2021**, *386*, 106016. [[CrossRef](#)]
50. Walshe, J.L. A six-component chlorite solid solution model and the conditions of chlorite formation in hydrothermal and geothermal systems. *Econ. Geol.* **1986**, *81*, 681–703. [[CrossRef](#)]
51. Charles, R.W.; Janecky, D.R.; Goff, F.; McKibben, M.A. Chemographic and Thermodynamic Analysis of the Paragenesis of the Major Phases in the Vicinity of the 6120-Foot (1866 m) Flow Zone, California State Well 2–14. *J. Geophys. Res. Solid Earth* **1988**, *93*, 13145–13157. [[CrossRef](#)]
52. Cho, M.; Liou, J.G.; Bird, D.K. Prograde phase relations in the State 2–14 well metasandstones, Salton Sea geothermal field, California. *J. Geophys. Res. Solid Earth* **1988**, *93*, 13081–13103. [[CrossRef](#)]
53. Barton, P.B.; Bethke, P.M.; Roedder, E. Environment of ore deposition in the Creede mining district, San Juan Mountains, Colorado; Part III, Progress toward interpretation of the chemistry of the ore-forming fluid for the OH Vein. *Econ. Geol.* **1977**, *72*, 1–24. [[CrossRef](#)]
54. Jacobs, D.C.; Parry, W.T. Geochemistry of biotite in the Santa Rita porphyry copper deposit, New Mexico. *Econ. Geol.* **1979**, *74*, 860–887. [[CrossRef](#)]
55. Luhr, J.F.; Carmichael, I.S.E.; Varekamp, J.C. The 1982 eruptions of El Chichón volcano, Chiapas, Mexico: Mineralogy and petrology of the anhydrite-bearing pumices. *J. Volcanol. Geotherm. Res.* **1984**, *23*, 69–108. [[CrossRef](#)]
56. Beryl, J.R.; Xavier, J.R. Halloysite for clay–polymer nanocomposites: Effects of nanofillers on the anti-corrosion, mechanical, microstructure, and flame-retardant properties—A review. *J. Mater. Sci.* **2023**, *58*, 10943–10974. [[CrossRef](#)]
57. Thomas, R.; Davidson, P.; Badanina, E. A melt and fluid inclusion assemblage in beryl from pegmatite in the Orlovka amazonite granite, East Transbaikalia, Russia: Implications for pegmatite-forming melt systems. *Mineral. Petrol.* **2009**, *96*, 129–140. [[CrossRef](#)]
58. Thomas, R.; Webster, J.D.; Davidson, P. Be-daughter minerals in fluid and melt inclusions: Implications for the enrichment of Be in granite–pegmatite systems. *Contrib. Mineral. Petrol.* **2011**, *161*, 483–495. [[CrossRef](#)]
59. Wones, D.R. Significance of the assemblage titanite+ magnetite+ quartz in granitic rocks. *Am. Miner.* **1989**, *74*, 744–749.
60. Gündüz, M.; Asan, K. MagMin_PT: An Excel-based mineral classification and geothermobarometry program for magmatic rocks. *Mineral. Mag.* **2023**, *87*, 1–9. [[CrossRef](#)]
61. Gerya, T.V.; Perchuk, L.L.; Triboulet, C.; Audren, C.; Sez’ko, A.I. Petrology of the Tumanshet Zonal Metamorphic Complex, Eastern Sayan. *Petrology* **1997**, *56*, 503–533.
62. Rybnikova, O.; Uher, P.; Novák, M.; Chládek, Š.; Bačík, P.; Kurylo, S.; Vaculovič, T. Chrysoberyl and associated beryllium minerals resulting from metamorphic overprinting of the Maršíkov–Schinderhübel III pegmatite, Czech Republic. *Mineral. Mag.* **2023**, *87*, 369–381. [[CrossRef](#)]
63. Abdalla, H.M. Mineralogical and geochemical characterization of beryl-bearing granitoids, Eastern Desert, Egypt: Metallogenic and exploration constraints. *Resour. Geol.* **2009**, *59*, 121–139. [[CrossRef](#)]
64. Saeseaw, S.; Renfro, N.D.; Palke, A.C.; Sun, Z.; McClure, S.F. Geographic origin determination of emerald. *Gems Gemol.* **2019**, *55*, 614–646. [[CrossRef](#)]
65. Schwarz, D. The Geographic Origin Determination of Emeralds. In *Color Special Issue*; International Colored Gemstone Association: Hong Kong; New York, NY, USA, 2015; pp. 98–105.
66. Bidny, A.S.; Baksheev, I.A.; Popov, M.P.; Anosova, M.O. Beryl from deposits of the Ural Emerald Belt, Russia: ICP-MS-LA and infrared spectroscopy study. *Mosc. Univ. Geol. Bull.* **2011**, *66*, 108–115. [[CrossRef](#)]
67. Neiva, A.M.; Neiva, J.M. Beryl from the granitic pegmatite at Namivo, Alto Ligonha, Mozambique. *Neues Jahrb. Mineral. -Abh.* **2005**, *181*, 173–182. [[CrossRef](#)] [[PubMed](#)]
68. Mokhtar, H.; Surour, A.A.; Azer, M.K.; Ren, M.; Said, A. New insights into chemical and spectroscopic characterization of beryl mineralization related to leucogranites in the west Wadi El Gemal area, southern Eastern Desert of Egypt. *Geochemistry* **2023**, *83*, 125980. [[CrossRef](#)]
69. Markl, G.; Schumacher, J.C. Beryl stability in local hydrothermal and chemical environments in a mineralized granite. *Am. Miner.* **1997**, *82*, 194–202. [[CrossRef](#)]
70. Beal, K.; Lentz, D.R.; Hall, D.C.; Dunning, G. Mineralogical, geochronological and geochemical characterization of Early Devonian aquamarine-bearing dykes of the Zealand Station beryl and molybdenite deposit, west central New Brunswick. *Can. J. Earth Sci.* **2010**, *47*, 859–874. [[CrossRef](#)]
71. Grundmann, G.; Morteani, G. Emerald Mineralization during Regional Metamorphism: The Habachtal (Austria) and Leydsdorp (Transvaal, South Africa) Deposits. *Econ. Geol.* **1989**, *84*, 835–849. [[CrossRef](#)]
72. Grundmann, G.; Morteani, G. Multi-stage emerald formation during Pan-African regional metamorphism: The Zabara, Sikait, Umm Kabo deposits, South Eastern desert of Egypt. *J. Afr. Earth Sci.* **2008**, *50*, 168–187. [[CrossRef](#)]

73. Grundmann, G.; Morteani, G. Emerald formation during regional metamorphism: The Zabara, Sikeit and Umm Kabo deposits (Eastern Desert, Egypt). In *Geoscientific Research in Northeast Africa*; CRC Press: Boca Raton, FL, USA, 2017; pp. 495–498.
74. Shinkankas, J. *Emerald and Other Beryls*; Chilton Book Co.: Randnor, PA, USA, 1981; p. 647.
75. Takla, M.A.; Surour, A.A.; Omar, S.A.M. Mapping, source of beryllium and genesis of some beryl occurrences in the Eastern Desert of Egypt. *Ann. Geol. Surv. Egypt* **2003**, *26*, 153–182.
76. Soliman, M.M. Ancient emerald mines and beryllium mineralization associated with Precambrian stanniferous granites in the Nugrus-Zabara Area, Southeastern Desert, Egypt. *Arab Gulf J. Sci. Res.* **1986**, *4*, 529–548.
77. Harraz, H.Z.; Hassan, A.M.; Furuyama, K. The Wadi Sikait Complex: A fertile post-collisional granite-pegmatite suite, Eastern Desert, Egypt. *Ann. Geol. Surv. Egypt* **2005**, *28*, 1–35.
78. Schwarz, D.; Giuliani, G. Emerald deposits—A review. *Aust. Gemmol.* **2001**, *21*, 17–23.
79. Mohamed, F.H.; Hassanen, M.A. Geochemistry and petrogenesis of Sikait leucogranite, Egypt: An example of Stype granite in a metapelitic sequence. *Geol. Rundsch.* **1997**, *86*, 81–92. [[CrossRef](#)]
80. Beus, A.A. Beryllium: Geochemistry of Beryllium and Genetic Types of Beryllium Deposits. AA Beus. translated by F. Lachman. Freeman, San Francisco, illus. \$15. *Science* **1966**, *154*, 1536.
81. Kovalenko, V.I.; Antipin, V.S.; Petrov, L.L. Distribution coefficients of Be in ongonites and some notes on its behavior in the rare metal lithium-fluorine granites. *Geochem. Int.* **1977**, *14*, 129–141.
82. Collins, W.J.; Beams, S.D.; White, A.J.R.; Chappell, B.W. Nature and origin of A-type granites with particular reference to southeastern Australia. *Contrib. Mineral. Petrol.* **1982**, *80*, 189–200. [[CrossRef](#)]
83. Whalen, J.B.; Currie, K.L.; Chappell, B.W. A-type granites: Geochemical characteristics, discrimination and petrogenesis. *Contrib. Mineral. Petrol.* **1987**, *95*, 407–419. [[CrossRef](#)]
84. Schwarz, D.; Giuliani, G.; Grundmann, G.; Glas, M. Die Entstehung der Smaragde, ein vieldiskutiertes Thema. In *Smaragd, der Kostbarste Beryll, der Teuerste Edelstein*; Schwarz, D., Hochlitner, R., Eds.; ExtraLapis: Charleston, SC, USA, 2001; pp. 68–73.
85. Omar, S.A. Mineralogical and fluid inclusions evidence for the genesis of Umm Addebbaa-Umm Kabu beryl belt, south Eastern Desert, Egypt. *Nucl. Sci. Sci. J.* **2016**, *5*, 1–14. [[CrossRef](#)]
86. Khaleal, F.M.; El-Bialy, M.Z.; Saleh, G.M.; Ibrahim, W.S.; El Dawy, M.N. The Geology, geochemistry and mineralogy of beryl mineralization in Zabara area, South Eastern Desert, Egypt. *Int. J. Miner. Sci.* **2019**, *5*, 18–34.
87. Hagag, W.; Moustafa, R.; Hamimi, Z. Neoproterozoic Evolution and Najd-Related Transpressive Shear Deformations Along Nugrus Shear Zone, South Eastern Desert, Egypt (Implications from Field-Structural Data and AMS-Technique). *Geotectonic* **2018**, *52*, 114–133. [[CrossRef](#)]
88. Abdalla, H.M.; Ishihara, S.; Matsueda, H.; Abdel-Monem, A.A. On the albite-enriched granitoids at Um Araarea, Southeastern Desert, Egypt. I) Geochemical, ore potentiality and fluid inclusion studies. *J. Geochem. Explor.* **1996**, *58*, 127–138. [[CrossRef](#)]
89. Schwartz, M.O. Geochemical criteria for distinguishing magmatic and metasomatic albite-enrichment in granitoids—Examples from the Ta-Li granite Yichun (China) and the Sn-W deposit Tikus (Indonesia). *Miner. Depos.* **1992**, *27*, 101–108. [[CrossRef](#)]
90. Aurisicchio, C.; Conte, A.M. Beryl from miarolitic pockets of granitic pegmatites, Elba, Italy: Characterization of crystal chemistry by means of EMP and SIMS analyses. *Can. Mineral.* **2012**, *50*, 1467–1488. [[CrossRef](#)]
91. Giuliani, G.; France-Lanord, C.; Cogez, P.; Schwarz, D.; Cheilletz, A.; Branquet, Y.; Giard, D.; Marrin-Izard, A.; Alexandrov, P.; Piat, D.H. Oxygen isotope systematics of emerald: Relevance for its origin and geological significance. *Miner. Depos.* **1998**, *33*, 315–319. [[CrossRef](#)]
92. Greiling, R.O.; Kroner, A.; El-Ramly, M.F.; Rashwan, A.A. Structural relationships between the Southern and Central parts of the Eastern Desert of Egypt: Details of a fold and thrust belt. In *The Pan-African Belt of Northeast Africa and Adjacent Areas: Tectonic Evolution and Economic Aspects of a Late Proterozoic Orogen*; El-Gaby, S., Greiling, R.O., Eds.; Friedr Vieweg: Berlin, Germany, 1988; pp. 121–145.
93. Ghoneim, M.F.; Lebda, E.M.; Nasr, B.B.; Khedr, M.Z. Geology and tectonic evolution of the area around wadi Arais, southern Eastern Desert, Egypt. In Proceedings of the 6th International Conference on the Geology of the Arab World (GAW6), Cairo, Egypt, 12 February 2002; Volume 1, pp. 45–66.
94. Heikal, M.T.S.; Khedr, M.Z.; El-Monesf, M.A.; Gomaa, S.R. Petrogenesis and geodynamic evolution of Neoproterozoic Abu Dabbab Albite Granite, Central Eastern Desert of Egypt: Petrological and geochemical constraints. *J. Afr. Earth Sci.* **2019**, *158*, 103518. [[CrossRef](#)]
95. Khedr, M.Z.; Abo Khashaba, S.M.; El-Shibiny, N.H.; El-Arafy, R.A.; Takazawa, E.; Azer, M.K.; Pallin, M. Remote sensing techniques and geochemical constraints on the formation of the Wadi El-Hima mineralized granites, Egypt: New insights into the genesis and accumulation of garnets. *Int. J. Earth Sci.* **2022**, *111*, 2409–2443. [[CrossRef](#)]
96. Khedr, M.Z.; Khashaba, S.M.A.; El-Shibiny, N.H.; Takazawa, E.; Hassan, S.M.; Azer, M.K.; Whattam, S.A.; El-Arafy, R.A.; Ichiyama, Y. Integration of remote sensing and geochemical data to characterize mineralized A-type granites, Egypt: Implications for origin and concentration of rare metals. *Int. J. Earth Sci.* **2023**, *112*, 1717–1745. [[CrossRef](#)]
97. Abo Khashaba, S.M.; El-Shibiny, N.H.; Hassan, S.M.; Takazawa, E.; Khedr, M.Z. Application of remote sensing data integration in detecting mineralized granitic zones: A case study of the Igla Ahmr, Central Eastern Desert, Egypt. *J. Asian Earth Sci.* **2023**, *200*, 104855.

98. Stern, J.R.; Khedr, Z.M.; Whitehouse, M.J.; Romer, R.L.; Abo Khashaba, S.M.; El-Shibiny, N.H. Late Cryogenian and early Ediacaran rare-metal rich granites in the Eastern Desert of Egypt: Constraints from zircon ages and whole-rock Sr- and Nd- and feldspar Pb-isotopic compositions. *J. Geol. Soc.* **2024**, *181*, jgs2023-068. [[CrossRef](#)]
99. Zwaan, J.C. Gemmology, geology and origin of the Sandawana emerald deposits, Zimbabwe. *Scr. Geol.* **2006**, *131*, 1–212.
100. Groat, L.A.; Giuliani, G.; Marshall, D.D.; Turner, D. Emerald deposits and occurrences: A review. *Ore Geol. Rev.* **2008**, *34*, 87–112. [[CrossRef](#)]

Disclaimer/Publisher’s Note: The statements, opinions and data contained in all publications are solely those of the individual author(s) and contributor(s) and not of MDPI and/or the editor(s). MDPI and/or the editor(s) disclaim responsibility for any injury to people or property resulting from any ideas, methods, instructions or products referred to in the content.